

A discontinuous stabilized mortar method for general 3D elastic problems

Patrice Hauret ^{a,*}, Patrick Le Tallec ^b

^a Manufacture Française des Pneumatiques Michelin, Centre de Technologies Ladoux, 63040 Clermont-Ferrand Cedex 9, France

^b Laboratoire de Mécanique des Solides, CNRS UMR 7649, Département de Mécanique, Ecole Polytechnique, 91128 Palaiseau Cedex, France

Received 12 November 2006; received in revised form 1 June 2007; accepted 18 June 2007

Available online 12 July 2007

Abstract

First, the present paper is concerned with the extension to linearized elastodynamics of the optimal results known in statics for the mortar method. It also analyzes and tests a new couple of displacements/Lagrange multipliers for the method, as proposed independently by Ben Belgacem [F. Ben Belgacem, A stabilized domain decomposition method with non-matching grids for the Stokes problem in three dimensions, *SIAM J. Numer. Anal.* 42 (2) (2004) 667–685] and the authors [P. Hauret, Méthodes numériques pour la dynamique des structures non-linéaires incompressibles à deux échelles (Numerical methods for the dynamic analysis of two-scale incompressible nonlinear structures), Ph.D. thesis, Ecole Polytechnique, 2004]. Finally, questions of practical implementation in the presence of curved interfaces are addressed and validated from the numerical point of view.

© 2007 Elsevier B.V. All rights reserved.

Keywords: Mortar methods; Discontinuous Lagrange multipliers; Stabilization; Curved interfaces

1. Introduction

Challenging industrial or biomechanical applications combine many substructures of different types and scales: surface rugosities, cracks, metallic grains, membranes, local reinforcements, soft inclusions, and so on. Each substructure has its own model, and discretization requirements. An efficient strategy for such applications is therefore to build independent approximations on each substructure and to implement coupling strategies handling displacement fields which are kinematically incompatible at the substructures interfaces.

In order to allow for such independent approximations by substructures, and to circumvent the drawbacks of point-wise matching among which a non-optimal convergence in “ \sqrt{h} ”, Bernardi et al. have introduced the mortar method [8,9]. The approach resorts to the imposition of the continu-

ity constraint at the interfaces under weak form. In [5], Ben Belgacem relaxes for the first time the constraint of strong continuity originally imposed on the boundary of interfaces, crucially improving the portability of the method to general 3D cases. This seminal achievement notwithstanding, the strategy retains two practical drawbacks of the original method. First, its flexibility remains limited by the compulsory modification of Lagrange multipliers on the boundary of interfaces where more than two domains meet. These cross points or cross lines may lead to noticeable complications in genuine three dimensional industrial applications, as observed in [7]. A possible solution was proposed in [31] when dealing with second-order approximation of the displacements at least. Indeed, Seshayier [31] has shown that provided an approximation of order $q \geq 2$ for the displacements is employed, Lagrange multipliers of order $q - 1$ suffice to preserve optimal convergence and do not require any modification in the vicinity of cross lines.

The second drawback of the original choice of Lagrange multipliers is a non-local coupling along interfaces. More precisely, for a locally supported function on the “master”

* Corresponding author.

E-mail addresses: hauret@cmapx.polytechnique.fr (P. Hauret), patrick.le-tallec@polytechnique.fr (P. Le Tallec).

side, the matching function on the slave side satisfying the weak continuity constraint will be possibly supported on the whole interface (see [36]). In other words, finding a matching function on the slave side of an interface requires the inversion of a fully coupled interface problem. To alleviate this restriction, Wohlmuth [36] and Kim et al. [23] have proposed the use of dual bases for Lagrange multipliers, which leads to a simple diagonal coupling enabling the efficient elimination of the weak continuity constraint. This philosophy has been successfully extended to higher order approximations [25], curved interfaces [18,19] and adapted to the formulation of contact problems [22]. Still, the compulsory modification of Lagrange multipliers at cross points remains an issue.

In order to preserve the advantages of locality of the dual approach and the computational flexibility of Seshaiyer's approach in 3D industrial problems, we develop and justify herein discontinuous stabilized mortar formulations. They were independently proposed by Ben Belgacem for the Stokes problem [6] and by Hauret and Le Tallec in [21] for elasticity and higher order approximations. They use discontinuous Lagrange multipliers of optimal order for the representation of interface fluxes, without modification at cross points. The price to pay for such a flexibility is to enrich the finite element space of admissible displacements by suitable interface bubble functions, following the ideas developed by Brezzi and Marini in the so-called three-field approach [15].

When confronted with industrial practice, there is still another practical problem to solve concerning the calculation of interface integrals and the treatment of curved interfaces. Indeed, the meshes of the subdomains are often generated separately and the initial interfaces of the decomposition are not exactly retained in the discrete model. More precisely, the geometry of the interface viewed by one subdomain will not be identical to the interface viewed by the facing subdomain. In such situations, the mortar method still lacks of a complete theoretical background beyond the 2D analysis performed by Flemisch et al. [17] and the adaption of dual Lagrange multipliers to this case [18,19]. A naive option consists in assembling the weak continuity constraint on the faceted non-mortar interface by simple projection of mortar displacements onto the non-mortar side element by element, but such a projection is not injective. Here, in order to preserve the theoretical convergence properties of the method and the smoothness of the interface, we propose an “exact” integration technique based on a smoothing interface procedure extended from Puso [28], continuing the works of Puso and Laursen [30,29].

In more details and using standard notation, the present paper will consider elastic problems in which one looks at each time t for the displacement field $u(t) \in H^1(\Omega)^3$ solution of the variational problem

$$\begin{cases} \int_{\Omega} \rho \ddot{u}(t) \cdot v + a_{\Omega}(u(t), v) = l(t; v) & \forall v \in H_*^1(\Omega)^3, \\ u = \bar{u} \quad \text{on } \Gamma_D. \end{cases} \quad (1)$$

Above, the space $H_*^1(\Omega) := \{v \in H^1(\Omega), \quad v|_{\Gamma_D} = 0\}$ is the space of kinematically admissible displacement fields where $\Gamma_D \subset \partial\Omega$ stands for the part of the boundary where displacements are prescribed. The standard elastic and potential (bi)linear forms are defined by

$$\begin{cases} a_{\Omega}(u, v) = \int_{\Omega} \mathbf{E}_{ijmn} \varepsilon(u)_{mn} \varepsilon(v)_{ij}, \\ l(v) = \int_{\Omega} f \cdot v + \int_{\Gamma_N} g \cdot v. \end{cases}$$

The elastic coefficients \mathbf{E}_{ijmn} satisfy the classical ellipticity and continuity constraints

$$\mathbf{E}_{ijmn}(x) \xi_{mn} \xi_{ij} \leq C_e \xi_{ij} \xi_{ij}, \quad \mathbf{E}_{ijmn}(x) \xi_{mn} \xi_{ij} \geq c_e \xi_{ij} \xi_{ij} \quad (2)$$

for almost every $x \in \Omega$ and every symmetric matrices $\xi, \zeta \in \mathbb{R}^{3 \times 3}$. The parameter c_e is proportional to the smallest Young modulus of the material present in Ω .

The present paper is organized as follows. Section 2 reviews the fundamental assumptions and convergence results arising when applying the mortar method to elasticity. Section 3 proposes a practical discontinuous stabilized formulation well-adapted to genuine 3D industrial problems and proves the *inf-sup* stability of the method. Section 4 is devoted to the practical adaption of the mortar constraint to the curved interface case, exploiting the Hermite regularization from Puso [28]. Finally, numerical examples aim at validating the proposed techniques on realistic 3D static and dynamic problems. The exact integration of the mortar constraint is also discussed from the numerical point of view.

2. Fundamental assumptions and convergence results

2.1. General setting

For simplicity, let us assume here that $\Omega \subset \mathbb{R}^3$ is a domain whose $(\Omega_k)_{1 \leq k \leq K}$ constitutes a partition into K subdomains. Each subdomain Ω_k , $1 \leq k \leq K$ corresponds to a particular substructure and is endowed with a family of finite element meshes $(\mathcal{T}_{k;h_k})_{h_k > 0}$, h_k denoting the maximum diameter of the elements of the local mesh $\mathcal{T}_{k;h_k}$. The corresponding finite element spaces of order $q \geq 1$ over Ω_k are denoted by

$$X_{k;h_k} = \{v \in H_*^1(\Omega_k)^3; \quad v|_K \in R_q(K)^3 \quad \forall K \in \mathcal{T}_{k;h_k}\} \oplus \mathcal{B}_{k;h_k}, \quad (3)$$

where $R_q(K)$ denotes the space of real-valued polynomials of degree less than or equal to q . The degree is a total degree when dealing with tetrahedral elements, i.e. $R_q(K) = P_q(K)$ with standard notation, and a partial degree when using iso-parametric hexahedral elements K , i.e. $R_q(K) = Q_q(K)$ with standard notation. Additionally, we have introduced a possible enrichment $\mathcal{B}_{k;h_k}$ that will be specified in the sequel. The resulting non-conforming approximation spaces in which looking for the displacement fields are then of the form

$$X_h = \{v \in L^2(\Omega)^3; \quad v|_{\Omega_k} \in X_{k;h_k}, \quad 1 \leq k \leq K\} \quad (4)$$

with $h = \max_{1 \leq k \leq K} h_k$.

Obviously, one has to enforce some matching conditions for the displacements at the interfaces between adjacent subdomains. Considering that pointwise matching has been proved in [8] to be suboptimal, following the early works from Bernardi et al. [8,9], and Ben Belgacem [5], we impose the continuity constraint at the interface under weak form and define the displacement space over Ω by

$$V_h = \left\{ v \in X_h; \int_{\Gamma_m} [v] \cdot \mu = 0, \mu \in M_{m;\delta_m}, 1 \leq m \leq M \right\}.$$

The sequence $(\Gamma_m)_{1 \leq m \leq M}$ is an enumeration of the interfaces $\partial\Omega_k \cap \partial\Omega_l$ when the domains Ω_k and Ω_l are adjacent, $1 \leq k < l \leq K$. Notation $[v]$ denotes the jump of $v \in X_h$ across the skeleton $\mathcal{S} = \cup_{1 \leq m \leq M} \Gamma_m$ and $M_{m;\delta_m} \subset L^2(\Gamma_m)^3$ a space of Lagrange multipliers to be defined below.

The elastic problems of interest will therefore be solved using discrete displacement fields belonging to V_h . Nevertheless, as $V_h \not\subset H_*^1(\Omega)^3$ the elastic bilinear form $a_\Omega : H_*^1(\Omega)^3 \times H_*^1(\Omega)^3 \rightarrow \mathbb{R}$ has to be extended to the product space X by

$$\tilde{a}(v, w) = \sum_{k=1}^K a_{\Omega_k}(u, v) \quad \forall u, v \in X = \prod_{k=1}^K H_*^1(\Omega_k)^3.$$

In order to obtain convergence results independent of the size of the different subdomains, X shall be endowed with the scaled broken Sobolev norm

$$\|v\|_X = \left(\sum_{k=1}^K \frac{1}{\text{diam}(\Omega_k)^2} \|v\|_{L^2(\Omega_k)^3}^2 + \|\nabla v\|_{L^2(\Omega_k)^3}^2 \right)^{1/2} \quad \forall v \in X.$$

The elastic problem therefore consists in finding at each discretization time t_{n+1} a displacement field $u_h^{n+1} \in V_h$ such that

$$\int_{\Omega} \rho \gamma_h^{n+\alpha} \cdot v_h + \tilde{a}(u_h^{n+\alpha}, v_h) = l(t_{n+\alpha}; v_h) \quad \forall v_h \in V_h. \quad (5)$$

Here $u_h^{n+\alpha} = u_h^n + \alpha(u_h^{n+1} - u_h^n)$ is a time interpolated value of the displacement field at time $t_{n+\alpha}$. The above general setting (5) can handle various constructions of the acceleration field $\gamma_h^{n+\alpha}$ as a function of the velocity field at time t_n and of the displacement field at times t_n and $t_{n+\alpha}$. For example, a first-order time implicit discretization will use $\alpha = 1$ and defines γ_h^{n+1} by

$$\begin{cases} \gamma_h^{n+1} = \frac{1}{\Delta t_n} (\dot{u}_h^{n+1} - \dot{u}_h^n), \\ \frac{1}{\Delta t_n} (u_h^{n+1} - u_h^n) = \dot{u}_h^{n+1}. \end{cases} \quad (6)$$

A standard trapezoidal rule uses $\alpha = 1/2$ and defines $\gamma_h^{n+1/2}$ by

$$\begin{cases} \gamma_h^{n+1/2} = \frac{1}{\Delta t_n} (\dot{u}_h^{n+1} - \dot{u}_h^n), \\ \frac{1}{\Delta t_n} (u_h^{n+1} - u_h^n) = \frac{1}{2} (\dot{u}_h^{n+1} + \dot{u}_h^n). \end{cases} \quad (7)$$

Static problems are simply obtained by setting $\gamma_h = 0$.

The mixed formulation of the above elastic problem (5) consists of finding $u_h^{n+1} \in X_h$ and $\lambda_\delta^{n+1} \in M_\delta := \prod_{m=1}^M M_{m;\delta_m}$ such that

$$\begin{cases} \int_{\Omega} \rho \gamma_h^{n+\alpha} \cdot v_h + \tilde{a}(u_h^{n+\alpha}, v_h) + b(v_h, \lambda_\delta^{n+1}) = l(t_{n+\alpha}; v_h) \\ \forall v_h \in X_h, \\ b(u_h^{n+1}, \mu_\delta) = 0 \quad \forall \mu_\delta \in M_\delta. \end{cases} \quad (8)$$

Above, we have introduced the bilinear form $b : X \times L^2(\mathcal{S})^3 \rightarrow \mathbb{R}$ defined by

$$b(v, \mu) = \sum_{m=1}^M \int_{\Gamma_m} [v] \cdot \mu \quad \forall (v, \mu) \in X \times L^2(\mathcal{S})^3, \quad (9)$$

whose kernel corresponds to the space V_h of discrete kinematically admissible displacement fields.

2.2. Fundamental assumptions

In the sequel, for each interface $\Gamma_m = \partial\Omega_k \cap \partial\Omega_l$ we introduce the non-mortar or slave side $k(m) := k$ or l chosen once for all and defining the interface space discretization. The mortar or master side is consequently $\bar{k}(m) := \{k, l\} \setminus k(m)$. The following trace spaces are then introduced:

$$W_{m;\delta_m} := \{v|_{\Gamma_m}; v \in X_{k(m);h_{k(m)}}\}, \quad W_{m;\delta_m}^0 := W_{m;\delta_m} \cap H_0^1(\Gamma_m)^3.$$

Those are the traces of finite element spaces built on the non-mortar side. In order to deal with the three dimensional case without severe restriction of conformity of the meshes on the boundary of the interfaces, we will use for analysis purpose the framework of mesh-dependent norms introduced by Agouzal and Thomas [1]. Following their definition, we denote:

$$\begin{aligned} \|v\|_{m;\frac{1}{2},\delta_m} &= \left(\sum_{F \in \mathcal{F}_{m;\delta_m}} \frac{1}{\text{diam}(F)} \|v\|_{L^2(F)}^2 \right)^{1/2}, \\ \|\mu\|_{m;-\frac{1}{2},\delta_m} &= \left(\sum_{F \in \mathcal{F}_{m;\delta_m}} \text{diam}(F) \|v\|_{L^2(F)}^2 \right)^{1/2}, \end{aligned}$$

in which the different F are the faces of the interface mesh $\mathcal{F}_{m;\delta_m}$ inherited from the mesh $\mathcal{T}_{k(m);h_{k(m)}}$ of the non-mortar subdomain $\Omega_{k(m)}$ facing Γ_m . In other words

$$\mathcal{F}_{m;\delta_m} = \{K \cap \Gamma_m; K \in \mathcal{T}_{k(m);h_{k(m)}}\}. \quad (10)$$

Consequently, the space M_δ of Lagrange multipliers shall be endowed with the following mesh-dependent norm:

$$\|\mu\|_{\delta,-\frac{1}{2}} = \left(\sum_{m=1}^M \|\mu\|_{m;-\frac{1}{2},\delta_m}^2 \right)^{1/2} \quad \forall \mu \in M_\delta,$$

and the space of traces with

$$\|w\|_{\delta,\frac{1}{2}} = \left(\sum_{m=1}^M \|w\|_{m;\frac{1}{2},\delta_m}^2 \right)^{1/2} \quad \forall w \in W_\delta := \prod_{m=1}^M W_{m;\delta_m}.$$

In order to obtain optimal stability and accuracy of the above discrete problems (8), several assumptions are required which we briefly review below (see for instance [37]). First, the aforementioned mixed formulations require [4,14,24] that $b(\cdot, \cdot)$ satisfies the *inf-sup* condition and that \tilde{a}

be coercive over the null-space of $b(\cdot, \cdot)$, i.e. V_h . In order to get convergence results independent of the chosen decomposition of Ω , and of the relative configuration of the adjacent meshes on interfaces, these conditions are assumed to be satisfied interface by interface and for conforming meshes. Indeed, the situation of conforming meshes is the most unfavorable from the point of view of the *inf-sup* condition, as the space of jumps on each interface is always richer than the traces of displacements on any side of the interface. The assumptions relative to the well-posedness of associated mixed problems are then the following.

Assumption 1 (*inf-sup condition*). For every $1 \leq m \leq M$, there exists a constant $\beta_m > 0$ independent of the mesh, such that

$$\inf_{\mu \in M_{m;\delta_m}} \sup_{w \in W_{m;\delta_m}^0 \setminus \{0\}} \frac{\int_{\Gamma_m} w \cdot \mu}{\|w\|_{m;\frac{1}{2},\delta_m} \|\mu\|_{m;-\frac{1}{2},\delta_m}} \geq \beta_m. \quad (11)$$

Remark 1. As proved in [37] for instance, Assumption 1 implies the existence of a constant $\beta > 0$ such that

$$\inf_{\mu \in M_\delta} \sup_{v \in X_h \setminus \{0\}} \frac{b(v, \mu)}{\|v\|_X \|\mu\|_{\delta, -\frac{1}{2}}} \geq \beta. \quad (12)$$

Assumption 2 (*coercivity*). For every $1 \leq m \leq M$, there exists a minimal Lagrange multiplier space \mathfrak{M}_m so that $\mathfrak{M}_m \subset M_{m;\delta_m}$ for all meshes. Moreover, \mathfrak{M}_m is such that every pair of local rigid body motions v_m and \bar{v}_m on $\Omega_{k(m)}$ and $\Omega_{\bar{k}(m)}$ respectively which satisfy the compatibility condition

$$\int_{\Gamma_m} (v_m - \bar{v}_m) \cdot \mu = 0 \quad \forall \mu \in \mathfrak{M}_m,$$

is strongly continuous on the interface : $v_m = \bar{v}_m$ on Γ_m .

Remark 2. Under Assumption 2, using a contradiction argument as in [8], one can prove that there exists an ellipticity constant $\tilde{\alpha} > 0$ such that

$$\tilde{a}(v, v) \geq \tilde{\alpha} \|v\|_X^2 \quad \forall v \in V, \quad (13)$$

where V stands for the constrained space of displacements associated with the minimal Lagrange multipliers spaces $(\mathfrak{M}_m)_{1 \leq m \leq M}$, i.e.

$$V = \left\{ v \in X; \int_{\Gamma_m} [v] \cdot \mu = 0, \mu \in \mathfrak{M}_m, 1 \leq m \leq M \right\}.$$

Consequently, as $V_h \subset V$, it follows that uniformly with respect to $h > 0$:

$$\tilde{a}(v_h, v_h) \geq \tilde{\alpha} \|v_h\|_X^2 \quad \forall v_h \in V_h.$$

Nevertheless, the argument gives no information on $\tilde{\alpha}$, and in particular, on its dependence on the number of subdomains, on their sizes, and on their shapes. This information though, remains crucial for domain decomposition methods as K is expected to become large. In the footsteps of

Gopalakrishnan [20] in the scalar case, Brenner has proved that the constant $\tilde{\alpha} > 0$ does not depend on the number, sizes and shapes of the subdomains [12,13]. The proof only holds for plane interfaces with further conditions on the Lagrange multipliers spaces $(\mathfrak{M}_m)_{1 \leq m \leq M}$. Under additional technical assumptions on the aspect ratio of the subdomains and the boundedness of curvatures, Hauret and Le Tallec have extended this result to curved interfaces [21, Section 4.4, p. 122].

Finally, when the continuous displacements u are sufficiently regular, namely each row of the stress tensor is locally in $H(\text{div}, \Omega_k)$ for all the subdomains Ω_k , $1 \leq k \leq K$, i.e. $(\mathbf{E} : \boldsymbol{\varepsilon}(u)) \in \prod_{k=1}^K H(\text{div}; \Omega_k)^3$, a simple application of Green's formula shows that Lagrange multipliers represent the normal forces at the interfaces:

$$\begin{aligned} \tilde{a}(u, v) - I(v) &= \sum_{k=1}^K \int_{\Omega_k} \mathbf{E}_{ijmn} \epsilon(u)_{mn} (\nabla v)_{ij} - \int_{\Omega} f \cdot v - \int_{\Gamma_N} g \cdot v \\ &= \sum_{m=1}^M \langle (\mathbf{E} : \boldsymbol{\varepsilon}(u)) \cdot v, [v] \rangle_{\Gamma_m} \quad \forall v \in X, \end{aligned} \quad (14)$$

where v stands for the normal unit vector on the skeleton \mathcal{S} in the direction where the jump $[\cdot]$ is counted positively; $\langle \cdot, \cdot \rangle_{\Gamma_m}$ denotes the duality product between $H^{1/2}(\Gamma_m)^3$ and its dual. Consequently, discrete spaces of Lagrange multipliers must be rich enough to represent this flux accurately, which leads to

Assumption 3 (*Accuracy*). Let q be the order of interpolation of the displacements as defined in (3). For every $1 \leq m \leq M$, discrete Lagrange multipliers must be such that

$$\inf_{\mu_\delta \in M_{m;\delta_m}} \|\lambda - \mu_\delta\|_{\delta, -\frac{1}{2}, m} \leq Ch_{k(m)}^q \|\lambda\|_{H^{q-\frac{1}{2}}(\Gamma_m)^3},$$

for a constant $C > 0$ independent of the mesh-sizes.

To counterbalance the practical advantage of mesh-dependent norms previously introduced, it is necessary to complement the above three assumptions by quasi-uniformity requirements on the local meshes:

Assumption 4 (*Quasi-uniformity*). For every $1 \leq m \leq M$, the family of interface meshes $(\mathcal{F}_{m;\delta_m})_{\delta_m > 0}$ obtained from the non-mortar side and defined by (10) is quasi-uniform. Moreover, denote by $\overline{\mathcal{F}}_{m;\overline{\delta}_m}$ the mesh of Γ_m obtained by replacing the non-mortar side by the mortar side in (10). We assume there exists a constant $C \geq 0$ independent of the mesh-sizes such that for every $1 \leq m \leq M$, we have

$$\text{diam}(\overline{F}) \leq C \text{ diam}(F) \quad \forall F \in \mathcal{F}_{m;\delta_m} \quad \forall \overline{F} \in \overline{\mathcal{F}}_{m;\overline{\delta}_m}.$$

2.3. Analysis

The analysis to be reviewed below is in fact restricted to situations with plane interfaces.

2.3.1. Static case

Under Assumptions 1 and 2, problem (8) is well-posed. Additionally, if we suppose Assumptions 3 and 4 to be satisfied, we obtain standard error estimates for the static problem (see [37,21]). The L^2 error estimate (17) will follow by a standard use of the Aubin–Nitsche argument [2]. Details can be found in [21, Lemma 4.12, p. 151]. In the sequel, we make use of the space

$$\mathbb{H}_E^{q+1}(\Omega) := \{v \in H^{q+1}(\Omega)^3, \quad \mathbf{E} : \boldsymbol{\varepsilon}(v) \in H^q(\Omega)^{3 \times 3}\},$$

endowed with the following semi-norm:

$$|u|_{q+1,E,\Omega}^2 = \|u\|_{H^{q+1}(\Omega)^3}^2 + \frac{1}{C_k^2} \|\mathbf{E} : \boldsymbol{\varepsilon}(u)\|_{H^q(\Omega)^{3 \times 3}}^2,$$

defined for any $u \in \mathbb{H}_E^{q+1}(\Omega)$. C_k is the constant C_e as defined in (2) over the subdomain Ω_k . Moreover, in view of justifying the use of the Aubin–Nitsche argument in the following theorem, we assume that Ω is regular enough so that for any loading $\phi \in [H_*^1(\Omega)]^3$, there exists a displacement field $\zeta_\phi \in \mathbb{H}_E^2(\Omega)$ such that

$$\tilde{a}(w, \zeta_\phi) = \langle \phi, w \rangle \quad \forall w \in H_*^1(\Omega).$$

Altogether, one can prove

Theorem 1. Under Assumptions 1–4, let $u \in \prod_{k=1}^K H^1(\Omega_k)^3$ be the solution of the static problem (1) written with $\rho = 0$ and let (u_h, λ_δ) be the solution of (8). If $(\mathbf{E} : \boldsymbol{\varepsilon}(u)) \in \prod_{k=1}^K H^q(\Omega_k)^{3 \times 3}$, $q \geq 1$, we have

$$\|u - u_h\|_{\tilde{a}}^2 \leq C \sum_{k=1}^K h_k^{2q} \left(C_k |u|_{H^{q+1}(\Omega_k)^3}^2 + \frac{1}{\tilde{\alpha}} \|\mathbf{E} : \boldsymbol{\varepsilon}(u)\|_{H^q(\Omega_k)^{3 \times 3}}^2 \right), \quad (15)$$

$$\|\lambda - \lambda_h\|_{\delta, -\frac{1}{2}} \leq C \left(1 + \frac{1}{\beta} \right) \|u - u_h\|_{\tilde{a}}, \quad (16)$$

$$\|u - u_h\|_{L^2(\Omega)^3}^2 \leq Ch^2 \sum_{k=1}^K C_k h_k^{2q} |u|_{q+1,E,\Omega_k}^2. \quad (17)$$

The energy norm $\|\cdot\|_{\tilde{a}}$ is defined by $\|v\|_{\tilde{a}} = \tilde{a}(v, v)^{1/2}$ for all $v \in X$. The constant $C > 0$ is independent of the number K , the size of the subdomains, and of the discretization; β is the inf–sup constant introduced in (12).

From the convergence analysis of the static problem, one can derive the convergence properties of the projection operator \mathbb{P}_h defined from $H_*^1(\Omega)$ onto V_h by

$$\tilde{a}(\mathbb{P}_h v, v_h) = \tilde{a}(v, v_h) \quad \forall v_h \in V_h, \quad \mathbb{P}_h v \in V_h.$$

In particular, the above theorem gives upper bound on the distance $\|v - \mathbb{P}_h v\|_{\tilde{a}}$ for smooth fields v .

2.3.2. Dynamic case

We generalize herein the static analysis to the dynamic problem (8) written with an arbitrary density $\rho > 0$. For the sake of clarity, we treat the first-order case (6) and refer to [21] for the technical details enabling the treatment of the second-order variant (7).

Proposition 1. Let $1 \leq r \leq q$, and

$$\begin{aligned} u &\in \mathcal{C}^1(0, T; \mathbb{H}_E^{q+1}(\Omega)) \cap \mathcal{C}^2\left(0, T; \prod_{k=1}^K \mathbb{H}_E^{r+1}(\Omega_k)^3\right) \\ &\cap \mathcal{C}^3(0, T; L^2(\Omega)^3) \\ \text{be solution of (1). If } (u_h^n, i_h^n)_{n \in \mathbb{N}} &\text{ is the fully discrete solution of (8), then the following error estimate holds:} \\ \int_{\Omega} \rho |\dot{u}_h^{n+1} - \dot{u}(t_{n+1})|^2 + \|u_h^{n+1} - u(t_{n+1})\|_{\tilde{a}}^2 &\leq C \left\{ \int_{\Omega} \rho |(id - \mathbb{P}_h)\dot{u}(0)|^2 + \|(id - \mathbb{P}_h)u(0)\|_{\tilde{a}}^2 \right. \\ &+ \Delta t^2 \|\rho\|_{L^\infty(\Omega)} \left(t_{n+1}^2 \|\ddot{u}\|_{C^0(0,T;L^2(\Omega)^3)}^2 + \|\ddot{u}\|_{C^0(0,T;L^2(\Omega)^3)}^2 \right) \\ &+ h^2 \|\rho\|_{L^\infty(\Omega)} \sum_{k=1}^K C_k h_k^{2r} \left(t_{n+1}^2 \|\ddot{u}\|_{C^0(0,T;\mathbb{H}_E^{r+1}(\Omega_k))}^2 \right. \\ &\left. \left. + \|\dot{u}\|_{C^0(0,T;\mathbb{H}_E^{r+1}(\Omega_k))} \right) + \frac{1}{\tilde{\alpha}} \sum_{k=1}^K C_k^2 h_k^{2q} \left(t_{n+1}^2 \|\dot{u}\|_{C^0(0,T;\mathbb{H}_E^{q+1}(\Omega_k))}^2 \right. \right. \\ &\left. \left. + \|u\|_{C^0(0,T;\mathbb{H}_E^{q+1}(\Omega_k))}^2 \right) \right\}. \end{aligned} \quad (18)$$

A similar convergence result was established by Azaiez et al. [3]. We mainly follow here the energetic approach from Le Tallec and Mani [35].

Proof. The proof is done in the case where Γ_D has a positive measure, but can be easily extended to a more general situation (cf. [21]). It is decomposed into four steps.

1. Evolution of error energy.

We introduce a new sequence of velocities $(v_h^n)_{n \in \mathbb{N}}$ deduced from the exact solution by

$$v_h^{n+1} = \frac{1}{\Delta t} (\mathbb{P}_h u(t_{n+1}) - \mathbb{P}_h u(t_n)). \quad (19)$$

Writing the dynamic problem (1) at time $t = t_{n+1}$ with test function $v_h \in V_h$ yields as in (14),

$$\begin{aligned} \int_{\Omega} \rho \frac{v_h^{n+1} - v_h^n}{\Delta t} \cdot v_h + \tilde{a}(u(t_{n+1}), v_h) &= l(t_{n+1}; v_h) \\ &+ \int_{\Omega} \rho \left(\frac{v_h^{n+1} - v_h^n}{\Delta t} - \ddot{u}(t_{n+1}) \right) \cdot v_h + \int_{\mathcal{S}} \lambda(t_{n+1}) \cdot [v_h]. \end{aligned} \quad (20)$$

Substracting to (20) the corresponding discrete time step (5), one obtains

$$\begin{aligned} \int_{\Omega} \rho \frac{ev_h^{n+1} - ev_h^n}{\Delta t} \cdot v_h + \tilde{a}(eu_h^{n+1}, v_h) &= \int_{\Omega} \rho \left(\frac{v_h^{n+1} - v_h^n}{\Delta t} - \ddot{u}(t_{n+1}) \right) \cdot v_h + \int_{\mathcal{S}} \lambda(t_{n+1}) \cdot [v_h], \end{aligned} \quad (21)$$

in which we have used the notation $ev_h^n = v_h^n - \dot{u}_h^n$ and $eu_h^n = \mathbb{P}_h u(t_n) - u_h^n$. Using $v_h = ev_h^{n+1}$ in (21), which coincides with $(eu_h^{n+1} - eu_h^n)/\Delta t$ by construction, and from the identity

$$\langle x^{n+1}, x^{n+1} - x^n \rangle = \frac{1}{2} |x^{n+1}|^2 - \frac{1}{2} |x^{n+1}|^2 + \frac{1}{2} |x^{n+1} - x^n|^2,$$

we obtain after summation over n and multiplication by Δt

$$\begin{aligned} \frac{1}{2} \int_{\Omega} \rho |ev_h^{n+1}|^2 + \frac{1}{2} \|eu_h^{n+1}\|_{\tilde{a}}^2 &\leq \frac{1}{2} \int_{\Omega} \rho |ev_h^0|^2 + \frac{1}{2} \|eu_h^0\|_{\tilde{a}}^2 \\ &+ \underbrace{\Delta t \sum_{i=0}^n \int_{\Omega} \rho \left(\frac{v_h^{i+1} - v_h^i}{\Delta t} - \ddot{u}(t_{i+1}) \right) \cdot ev_h^{i+1}}_{\text{I}} \\ &+ \underbrace{\sum_{i=0}^n \int_{\mathcal{S}} \lambda(t_{i+1}) \cdot [eu_h^{i+1} - eu_h^i]}_{\text{II}}. \end{aligned} \quad (22)$$

2. Approximation error.

Resorting to the Cauchy–Schwartz inequality, one gets the following bound for I, as introduced in (22):

$$\begin{aligned} I &\leq \frac{\Delta t}{\tau} \left(\tau^2 \sum_{i=0}^n \int_{\Omega} \rho \left| \frac{v_h^{i+1} - v_h^i}{\Delta t} - \ddot{u}(t_{i+1}) \right|^2 \right)^{1/2} \left(\sum_{i=0}^n \int_{\Omega} \rho |ev_h^{n+1}|^2 \right)^{1/2} \\ &\leq \frac{\Delta t}{2\tau} \left(\tau^2 \sum_{i=0}^n \int_{\Omega} \rho \left| \frac{v_h^{i+1} - v_h^i}{\Delta t} - \ddot{u}(t_{i+1}) \right|^2 \right) \\ &\quad + \frac{\Delta t}{2\tau} \left(\sum_{i=0}^n \int_{\Omega} \rho |ev_h^{n+1}|^2 \right), \end{aligned}$$

where τ denotes a reference time scale. By construction, we have $(v_h^{i+1} - v_h^i)/\Delta t = \mathbb{P}_h(u(t_{i+1}) - 2u(t_i) + u(t_{i-1}))/\Delta t^2 =: \mathbb{P}_h \gamma_i$. Using Taylor expansion and (15), we get

$$\begin{aligned} I &\leq \frac{\Delta t}{\tau} \left(\tau^2 \sum_{i=0}^n \int_{\Omega} \rho |\gamma_i - \ddot{u}(t_{i+1})|^2 \right) \\ &\quad + \frac{\Delta t}{\tau} \left(\tau^2 \sum_{i=0}^n \int_{\Omega} \rho |\mathbb{P}_h \gamma_i - \gamma_i|^2 \right) + \frac{\Delta t}{2\tau} \left(\sum_{i=0}^n \int_{\Omega} \rho |ev_h^{n+1}|^2 \right) \\ &\leq \frac{T}{\tau} \left(\Delta t^2 \|\rho\|_{L^\infty(\Omega)} \|\tau \ddot{u}\|_{L^\infty(0,T;L^2(\Omega)^3)}^2 \right) \\ &\quad + C \frac{T}{\tau} \left(h^2 \|\rho\|_{L^\infty(\Omega)} \sum_{k=1}^K \mathfrak{C}_k h_k^{2r} \sup_{t \in [0,T]} |\tau \ddot{u}(t)|_{r+1,\mathbf{E},\Omega_k}^2 \right) \\ &\quad + \frac{\Delta t}{2\tau} \left(\sum_{i=0}^n \int_{\Omega} \rho |ev_h^{n+1}|^2 \right). \end{aligned}$$

3. Consistency error.

A discrete integration by parts of the error term II yields

$$\begin{aligned} \text{II} &= - \underbrace{\sum_{i=1}^{n-1} \int_{\mathcal{S}} (\lambda(t_{i+1}) - \lambda(t_i)) \cdot [eu_h^i]}_{\text{III}} + \underbrace{\int_{\mathcal{S}} \lambda(t_{n+1}) \cdot [eu_h^{n+1}]}_{\text{IV}} \\ &\quad - \underbrace{\int_{\mathcal{S}} \lambda(t_1) \cdot [eu_h^0]}_{\text{V}}. \end{aligned}$$

Since $eu_h^i \in V_h$, we obtain for every $\mu_\delta \in M_\delta$ the following bound of the term III by using the Cauchy–Schwartz inequality and the Sobolev trace theorem:

$$\begin{aligned} |\text{III}| &= \left| \frac{\Delta t}{\tau} \sum_{i=1}^{n-1} \int_{\mathcal{S}} \left(\tau \frac{\lambda(t_{i+1}) - \lambda(t_i)}{\Delta t} - \mu_\delta \right) \cdot [eu_h^i] \right| \\ &\leq \frac{\Delta t}{2\tau} \Theta \sum_{i=1}^{n-1} \int_{\mathcal{S}} \left| \tau \frac{\lambda(t_{i+1}) - \lambda(t_i)}{\Delta t} - \mu_\delta \right|^2 + \frac{\Delta t}{2\tau} \Theta^{-1} \sum_{i=1}^{n-1} \|eu_h^i\|_X^2, \end{aligned}$$

where $\Theta > 0$ is arbitrary. Let us select $\Theta^{-1} = \tilde{\alpha}$ where $\tilde{\alpha}$ is the coercivity constant defined in (13). Assumption 3, Taylor's expansion and the Sobolev trace theorem imply that

$$\begin{aligned} |\text{III}| &\leq C \frac{\Delta t}{2\tilde{\alpha}\tau} \sum_{i=1}^{n-1} \sum_{m=1}^M h_{k(m)}^{2q} \|\tau \dot{\lambda}\|_{L^\infty(0,T;H^{q-\frac{1}{2}}(\Gamma_m)^3)}^2 \\ &\quad + \frac{\Delta t}{2\tau} \sum_{i=1}^{n-1} \|eu_h^i\|_{\tilde{a}}^2 \\ &\leq C \frac{T}{2\tilde{\alpha}\tau} \sum_{k=1}^K \mathfrak{C}_k^2 h_k^{2q} \sup_{t \in [0,T]} |\tau \dot{u}|_{q+1,\mathbf{E},\Omega_k}^2 + \frac{\Delta t}{2\tau} \sum_{i=1}^{n-1} \|eu_h^i\|_{\tilde{a}}^2. \end{aligned}$$

Similarly, one obtains

$$\begin{aligned} |\text{IV}| &\leq C \sum_{k=1}^K \mathfrak{C}_k^2 h_k^{2q} \sup_{t \in [0,T]} |u(t)|_{q+1,\mathbf{E},\Omega_k}^2 + \frac{1}{4} \|eu_h^{n+1}\|_{\tilde{a}}^2, \\ |\text{V}| &\leq C \sum_{k=1}^K \mathfrak{C}_k^2 h_k^{2q} \sup_{t \in [0,T]} |u(t)|_{q+1,\mathbf{E},\Omega_k}^2 + \frac{1}{4} \|eu_h^0\|_{\tilde{a}}^2. \end{aligned}$$

4. Conclusion.

Plugging the above estimates of I and II into (22) implies

$$\begin{aligned} \frac{1}{2} \left(1 - \frac{\Delta t}{\tau} \right) \int_{\Omega} \rho |ev_h^{n+1}|^2 + \frac{1}{4} \|eu_h^{n+1}\|_{\tilde{a}}^2 &\leq \frac{1}{2} \int_{\Omega} \rho |ev_h^0|^2 \\ &\quad + \frac{3}{8} \|eu_h^0\|_{\tilde{a}}^2 + \frac{T}{\tau} \left(\Delta t^2 \|\rho\|_{L^\infty(\Omega)} \|\tau \ddot{u}\|_{L^\infty(0,T;L^2(\Omega)^3)}^2 \right) \\ &\quad + C \frac{T}{\tau} \left(h^2 \|\rho\|_{L^\infty(\Omega)} \sum_{k=1}^K \mathfrak{C}_k h_k^{2r} \sup_{t \in [0,T]} |\tau \ddot{u}(t)|_{r+1,\mathbf{E},\Omega_k}^2 \right) \\ &\quad + C \frac{T}{2\tilde{\alpha}\tau} \sum_{k=1}^K \mathfrak{C}_k^2 h_k^{2q} \sup_{t \in [0,T]} (|\tau \dot{u}(t)|_{q+1,\mathbf{E},\Omega_k}^2) + \sup_{t \in [0,T]} (|u(t)|_{q+1,\mathbf{E},\Omega_k}^2) \\ &\quad + \frac{\Delta t}{2\tau} \left(\sum_{i=0}^{n-1} \int_{\Omega} \rho |ev_h^{n+1}|^2 \right) + \frac{\Delta t}{2\tau} \sum_{i=1}^{n-1} \|eu_h^i\|_{\tilde{a}}^2. \end{aligned} \quad (23)$$

A discrete version of the Gronwall's lemma (see for instance [21, Lemma 4.13, p. 175]) implies for $\Delta t \leq \tau/2$ that

$$\begin{aligned} \int_{\Omega} \rho |ev_h^{n+1}|^2 \cdot v_h + \|eu_h^{n+1}\|_{\tilde{a}}^2 &\leq C \frac{T}{\tau} \left\{ \int_{\Omega} \rho |ev_h^0|^2 + \|eu_h^0\|_{\tilde{a}}^2 \right. \\ &\quad + \left(\Delta t^2 \|\rho\|_{L^\infty(\Omega)} \|\tau \ddot{u}\|_{L^\infty(0,T;L^2(\Omega)^3)}^2 \right) \\ &\quad + \left(h^2 \|\rho\|_{L^\infty(\Omega)} \sum_{k=1}^K \mathfrak{C}_k h_k^{2r} \sup_{t \in [0,T]} |\tau \ddot{u}(t)|_{r+1,\mathbf{E},\Omega_k}^2 \right) \\ &\quad + \frac{1}{\tilde{\alpha}} \sum_{k=1}^K \mathfrak{C}_k^2 h_k^{2q} \sup_{t \in [0,T]} (|\tau \dot{u}(t)|_{q+1,\mathbf{E},\Omega_k}^2) + \sup_{t \in [0,T]} (|u(t)|_{q+1,\mathbf{E},\Omega_k}^2) \\ &\quad \times \left. \left(1 + \frac{\Delta t}{2\tau} \right)^{n+1} \right\}. \end{aligned} \quad (24)$$

Observe we can choose $T = \tau = t_{n+1}$, and doing so, the factor

$$\left(1 + \frac{\Delta t}{2t_{n+1}} \right)^{n+1} = \exp \left(\frac{t_{n+1}}{\Delta t} \log \left(1 + \frac{\Delta t}{2t_{n+1}} \right) \right)$$

remains bounded by \sqrt{e} independently of Δt and t_{n+1} . The final result follows from the triangular inequality

$$\|u(t_{n+1}) - u_h^{n+1}\|_{\tilde{a}} \leq \|u(t_{n+1}) - \mathbb{P}_h u(t_{n+1})\|_{\tilde{a}} + \|e u_h^{n+1}\|_{\tilde{a}}, \quad (25)$$

and from the decomposition

$$\begin{aligned} \|\dot{u}(t_{n+1}) - \dot{u}_h^{n+1}\|_{L^2(\Omega)^3} &\leq \|\dot{u}(t_{n+1}) - \mathbf{v}_h^{n+1}\|_{L^2(\Omega)^3} \\ &+ \|\mathbf{v}_h^{n+1} - \mathbb{P}_h \mathbf{v}_h^{n+1}\|_{L^2(\Omega)^3} + \|e v_h^{n+1}\|_{L^2(\Omega)^3}, \end{aligned} \quad (26)$$

with $\mathbf{v}_{n+1} = (u(t_{n+1}) - u(t_n)) / \Delta t$. \square

3. A discontinuous stabilized formulation

In this section, we introduce special choices of discontinuous Lagrange multipliers which do not require any special treatment at cross points or cross lines. At the same time, the locality of the proposed formulation is improved in the sense that the coupling matrix is block diagonal. This choice meets all the requirements of Assumptions 1–3. The construction relies on the following basic choice of discontinuous local Lagrange multipliers:

$$M_{m;\delta_m} = \{\mu \in L^2(\Gamma_m)^3; \mu|_F \in \mathcal{P}_{q-1}(F)^3 \forall F \in \mathcal{F}_{m;\delta_m}\}. \quad (27)$$

This choice obviously satisfies Assumption 3. The price to pay in order to verify the *inf-sup* condition (Assumption 1) is the addition of a stabilization in the form of the enrichment $\mathcal{B}_{k;h_k}$ in (3) (see Fig. 1).

3.1. First-order case $q = 1$

3.1.1. Setting and analysis

The interface flux is approximated here by piecewise constants. For any face $F \in \mathcal{F}_{m;\delta_m}$, let $K(F)$ stand for the non-mortar element having F as a face. We propose to enrich the space of displacements by a single interface bubble b_F defined as follows. If $K(F)$ is a tetrahedron whose vertices are denoted by $(a_i)_{1 \leq i \leq 4}$ with the associated barycentric coordinates $(\lambda_i)_{1 \leq i \leq d+1}$, the interface bubble b_F can be defined (see Fig. 1) as:

$$b_F = \prod_{a_i \in F} \lambda_i.$$

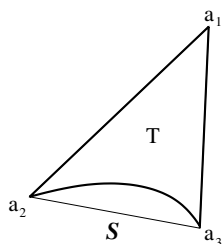


Fig. 1. Bubble function $\lambda_2 \lambda_3$ on the interface \mathcal{S} , in a triangle T (2D case).

When considering a cubic reference element $\hat{Q} = [-1, 1]^3$, we can also define the face bubble associated with the face $\hat{F} = [-1, 1]^2 \times \{-1\}$ by

$$b_{\hat{F}} = \frac{1}{2}(1-x_1^2)(1-x_2^2)(1-x_3) \quad \forall \hat{x} = (\hat{x}_1, \hat{x}_2, \hat{x}_3) \in [-1, 1]^3.$$

For this choice, we have

Proposition 2. Let $M_{m;\delta_m}$ be defined by (27) for every $1 \leq m \leq M$. Let X_h be the space of displacements defined by (4) for $q = 1$ and enriched with the aforementioned interface bubbles. Then, Assumption 1 holds with a stability constant independent of the discretization.

Proof. The proof will build a mapping $\pi_m : L^2(\Gamma_m)^3 \rightarrow W_{m;\delta_m}^0$ such that for every $w \in L^2(\Gamma_m)^3$, we have

$$\begin{cases} \int_{\Gamma_m} \pi_m w \cdot \mu = \int_{\Gamma_m} w \cdot \mu \quad \forall \mu \in M_{m;\delta_m}, \\ \|\pi_m w\|_{m,\delta_m,\frac{1}{2}} \leq C_m \|w\|_{m,\delta_m,\frac{1}{2}}. \end{cases} \quad (28)$$

Such a relation clearly implies inequality (11) with $\beta_m = C_m^{-1}$.

To check (28), let I_m be an interpolation operator from $L^2(\Gamma_m)^3$ to $W_{m;\delta_m}^0$. For all $w \in L^2(\Gamma_m)^3$, we define

$$\pi_m w = I_m w + \sum_{F \in \mathcal{F}_{m;\delta_m}} \gamma_F b_F \Big|_F$$

with $(\gamma_F)_{F \in \mathcal{F}_{m;\delta_m}}$ a set of coefficients to be defined below. Because Lagrange multipliers are piecewise constant, satisfying the first line in (28) implies that for all $F \in \mathcal{F}_{m;\delta_m}$ we must have

$$\int_F \pi_m w = \int_F w,$$

which imposes

$$\gamma_F = \frac{\int_F w - I_m w}{\int_F b_F}. \quad (29)$$

Let us now show that $\int_F b_F \geq C \text{ meas}(F)$. If the mesh is affine, a classical change of variable onto the reference element \hat{F} provides

$$\int_F b_F = \frac{\text{meas}(F)}{\text{meas}(\hat{F})} \int_{\hat{F}} \hat{b} = C \text{ meas}(F).$$

Let us now assume the mesh is a general quadrangular mesh. We denote by $J_F \in \mathbb{Q}_1(\hat{F})^3$ the mapping between the reference square \hat{F} and the non-mortar face F rescaled by the homothety ratio $1/\text{diam}(\Omega)$ and centered at the origin $0 \in \mathbb{R}^3$. Let us introduce $\mathcal{J} = \{J_F, F \in \mathcal{F}_{m;\delta_m}\}$. Observe $\mathcal{J} \subset \mathbb{Q}_1(\hat{F})^3$ is bounded in a finite dimension space uniformly with respect to the mesh-size; it is therefore compact. Additionally, the mapping

$$\mathcal{A} : J \in \mathcal{J} \mapsto \frac{1}{\text{meas}(J(\hat{F}))} \int_{J(\hat{F})} b_{J(\hat{F})} \in \mathbb{R}_+^*$$

is continuous and since \mathcal{J} is compact, \mathcal{A} reaches its bounds. As a consequence, there exists a constant $C > 0$

independent of the mesh-size such that $\int_F b_F \geq C \text{ meas}(F)$ for all $F \in \mathcal{F}_{m;\delta_m}$, $1 \leq m \leq M$.

Consequently, (29) and the Cauchy–Schwartz inequality yield

$$|\gamma_F| \leq C \frac{\|w - I_m w\|_{L^2(F)}}{\text{meas}(F)^{1/2}}.$$

Thus, we obtain the following estimate:

$$\begin{aligned} \|\pi_k w\|_{\delta_{\frac{1}{2},m}}^2 &= \sum_{F \in \mathcal{F}_{m;\delta_m}} \frac{1}{h(F)} \|\pi_k w\|_{L^2(F)}^2 \leq C \left(\sum_{F \in \mathcal{F}_{m;\delta_m}} \frac{1}{h(F)} \|I_m w\|_{L^2(F)}^2 \right. \\ &\quad \left. + \sum_{F \in \mathcal{F}_{m;\delta_m}} \frac{1}{h(F)} \|w - I_m w\|_{L^2(F)}^2 \frac{\|b_F\|_{L^2(F)}^2}{\text{meas}(F)} \right) \\ &\leq C \left(\sum_{F \in \mathcal{F}_{m;\delta_m}} \frac{1}{h(F)} \|I_m w\|_{L^2(F)}^2 \right. \\ &\quad \left. + \sum_{F \in \mathcal{F}_{m;\delta_m}} \frac{1}{h(F)} \|w - I_m w\|_{L^2(F)}^2 \right) \\ &\leq C \left(\sum_{F \in \mathcal{F}_{m;\delta_m}} \frac{1}{h(F)} \|I_m w\|_{L^2(F)}^2 + \sum_{F \in \mathcal{F}_{m;\delta_m}} \frac{1}{h(F)} \|w\|_{L^2(F)}^2 \right). \end{aligned}$$

By choosing the interpolation operator I_m as the projection from $L^2(\Gamma_m)^3$ to $W_{m;\delta_m}^0$ for the inner product

$$\langle u, v \rangle_{\delta_{\frac{1}{2},m}} = \sum_{F \in \mathcal{F}_{m;\delta_m}} \frac{1}{h(F)} \int_F u \cdot v,$$

which ensures $\|I_m w\|_{m,\delta_{m,\frac{1}{2}}} \leq \|w\|_{m,\delta_{m,\frac{1}{2}}}$, we conclude that $\|\pi_m w\|_{\delta_{\frac{1}{2},m}} \leq C \|w\|_{\delta_{\frac{1}{2},m}}$, ending the proof. \square

Finally, it is not difficult to show that the proposed formulation satisfies Assumption 2, at least for plane interfaces decomposed into four quadrilateral parts. More precisely, we state (see [21, Lemma 4.3, p. 117] for a detailed proof):

Proposition 3. Assume that $\Gamma_m = \partial\Omega_k \cap \partial\Omega_l$ is plane and is the image of a reference quadrilateral

$$\Gamma_m := \left\{ x \in \mathbb{R}^3; \quad x - G_m = \sum_{l=1}^2 \xi_l e_l, \quad \xi_l \in [-1; 1] \right\},$$

where $G_m = |\Gamma_m|^{-1} \int_{\Gamma_m} x \, dx$ is the barycenter of Γ_m . By construction, Γ_m can be splitted into four parts $(\gamma_j^m)_{1 \leq j \leq 4}$ where $\xi_l \in [-1; 0]$ or $\xi_l \in [0; 1]$ for every $1 \leq l \leq 2$ (see Fig. 2). Then the Lagrange multiplier space

$$\mathfrak{M}_m = \left\{ \mu \in L^2(\Gamma_m)^3; \quad \mu|_{\gamma_j^m} \text{ is a constant, } 1 \leq j \leq 4 \right\}$$

will satisfy Assumption 2.

3.1.2. Counter-example and numerical validation

We show here that Assumption 1 can be easily violated when a bubble stabilization is not introduced. For example, let us consider an interface \mathcal{S} whose non-mortar side is represented in Fig. 3, and equipped with a uniform square mesh. The diameter of the squares is denoted by δ .

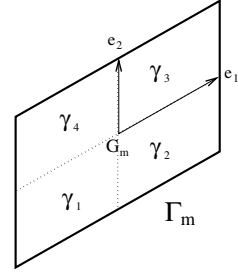


Fig. 2. Decomposition of Γ_m and construction of the minimal Lagrange multiplier space \mathfrak{M}_m .

We adopt the classical $\mathbb{Q}_1 \times \mathbb{P}_0$ discretization:

$$\begin{cases} M_\delta = \{p \in L^2(\mathcal{S})^3, \quad p|_F \in \mathbb{P}_0(F)^3 \quad \forall F \in \mathcal{F}_\delta\}, \\ W_\delta^0 = \{p \in H_0^1(\mathcal{S})^3 \cap \mathcal{C}^0(\mathcal{S})^3, \quad p|_F \in \mathbb{Q}_1(F)^3 \\ \quad \forall F \in \mathcal{F}_\delta\}. \end{cases}$$

If $\lambda_h^* \in M_\delta$ is taken as a “checker board”, i.e.

$$\lambda_h^*|_F = \pm a, \quad a \in \mathbb{R}^3$$

depending of $F \in \mathcal{F}_\delta$ in the way indicated by Fig. 3, then we have by symmetry of each shape function with respect to each node,

$$\int_{\mathcal{S}} \phi_h \cdot \lambda_h^* = 0 \quad \forall \phi_h \in W_\delta^0.$$

As a consequence, Assumption 1 is not satisfied.

Remark 3. The standard Assumption 1 ensures the well-posedness of the approximate problem (8) independently of the relative configuration of the mortar and non-mortar meshes. In particular, it is always strictly stronger than the inf–sup condition (12), except in the conforming case, where it is equivalent. The instability shown in Fig. 3 entails that (8) is not well-posed for conforming meshes on the interface, but the problem (8) could be well-posed for strictly non-conforming interfaces. Indeed, in the inf–sup condition (12), the displacement over the interface enters through its jump whereas it only enters in Assumption 1 through its value on the non-mortar side. Obviously, the space of jumps over the interface can be considerably richer

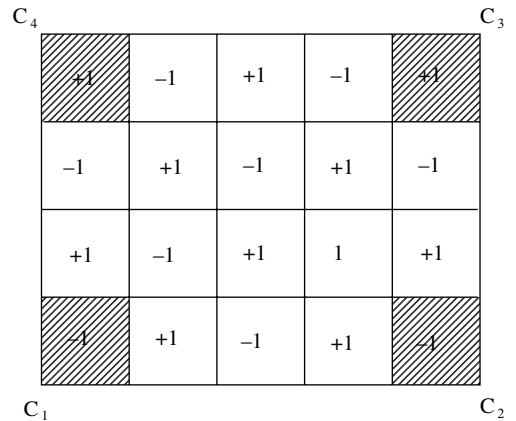


Fig. 3. Uniform square mesh of the interface \mathcal{S} between two subdomains.

than the space of the displacements on the non-mortar side if the interface is really non-conforming. This enrichment coming from the non-conformity can make the inf-sup condition (12) satisfied, but in such case, there will be no robustness with respect to the relative position of the interfaces.

In any case, as soon as a bubble stabilization is introduced, the inf-sup constant β_m in Assumption 1 remains strictly positive independently of the discretization.

3.2. Second-order case $q = 2$

3.2.1. Macro-element analysis

The macro-element analysis of Boland–Nicolaides [10,11] and Stenberg [32–34] is a practical way of verifying the inf-sup condition. Its extension to the mortar framework is rather straightforward and we refer to [21, Lemma 4.15, p. 475] for the details. The assumptions follow. Assume that for every $1 \leq m \leq M$, the interface Γ_m is equipped with a family of macro-meshes $(\mathcal{N}_{m;\delta_m})_{\delta_m > 0}$. Each macro-element $\omega \in \mathcal{N}_{m;\delta_m}$ is a subset $\omega \subset \mathcal{F}_{m;\delta_m}$ of adjacent elements. We assume that

- (1) every element $F \in \mathcal{F}_{m;\delta_m}$ belongs to at least one macro-element and less than L macro-elements, independently of the mesh-size δ_m ,
- (2) each $\omega = \cup_i F_i \in \mathcal{N}_{m;\delta_m}$ is the image of a reference macro-element $\hat{\omega} = \cup_i \hat{F}_i \in \hat{\mathcal{N}}$ by an homeomorphism J such that $J|_{\hat{F}_i} : \hat{F}_i \rightarrow F_i$ is one-to-one; the reference macro-element $\hat{\mathcal{N}}$ has a bounded number of reference elements, independently of the mesh-size δ_m ,
- (3) for every $\hat{\omega} \in \hat{\mathcal{N}}$, for every $\hat{\mu} \in M(\hat{\omega})$ such that

$$\int_{\hat{\omega}} \hat{w} \cdot \hat{\mu} = 0 \quad \forall \hat{w} \in W^0(\hat{\omega}) \text{ we must have } \hat{\mu} = 0. \quad (30)$$

The spaces $W^0(\hat{\omega})$ and $M(\hat{\omega})$ constructed on $\hat{\omega}$ are the counterparts on $\hat{\omega}$ of the spaces $W_{m;\delta_m}^0$ and $M_{m;\delta_m}$ constructed on Γ_m .

The result reads

Proposition 4. *Assume that for every $1 \leq m \leq M$, the aforementioned statements (1)–(3) are satisfied. Then, Assumption 1 is true with constants independent of δ_m .*

In the sequel, we apply this technique to the verification of the inf-sup stability condition for discontinuous stabilized formulations using higher order approximations. The proof uses macro-elements made of single elements. Observe this is much more powerful than just checking for $\mu \in M_{m;\delta_m}$ that

$$\int_{\Gamma_m} w \cdot \mu = 0 \quad \forall w \in W_{m;\delta_m} \Rightarrow \mu = 0.$$

Indeed, the “macro-element” checking ensures independence of the inf-sup constant with respect to the mesh.

3.2.2. Hexaedral elements

Let $\hat{Q} = [-1; 1]^3 = \hat{\omega} \times [-1; 1]$ be the reference cube whose $\hat{\omega} \times \{-1\}$ is a face included in the non-conforming interface. To stabilize the second-order displacements $\mathbb{Q}_2(\hat{Q})^3$, two interface bubbles are required, given along each geometric direction by

$$\begin{aligned} \hat{b}_1(x_1, x_2, x_3) &= x_1(1 - x_1^2)(1 - x_2^2)(1 - x_3), \\ \hat{b}_2(x_1, x_2, x_3) &= x_2(1 - x_1^2)(1 - x_2^2)(1 - x_3). \end{aligned}$$

The trace of such bubble functions on the interface $\hat{\omega}$ is illustrated in Fig. 4. Checking implication (30) is elementary (the reader is referred to [21, p. 179] for further details).

3.2.3. Tetrahedral elements

Let \hat{T} be a reference tetrahedron whose nodes are denoted by $(a_i)_{1 \leq i \leq 4}$ and the corresponding barycentric coordinates by $(\lambda_j)_{1 \leq j \leq 4}$. We assume that a_4 does not belong to the face $\hat{\omega}$ of \hat{T} which is included in the non-conforming interface. The standard second order displacements $\mathbb{P}_2(\hat{T})^3$ are enriched by three bubbles, generated along each geometric direction by

$$\begin{aligned} \hat{b}_1 &= \left(\lambda_1 - \frac{1}{2} \right) \lambda_1 \lambda_2 \lambda_3 \lambda_4, \\ \hat{b}_2 &= \left(\lambda_2 - \frac{1}{2} \right) \lambda_1 \lambda_2 \lambda_3 \lambda_4, \\ \hat{b}_3 &= \left(\lambda_3 - \frac{1}{2} \right) \lambda_1 \lambda_2 \lambda_3 \lambda_4. \end{aligned}$$

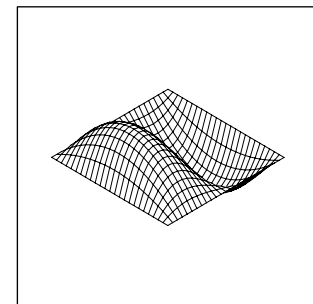


Fig. 4. The trace of the bubble function \hat{b}_1 on the face $\hat{\omega}$ of the reference cube \hat{Q} . Of course \hat{b}_2 is obtained by permutation of the two coordinates $(x_1; x_2)$.

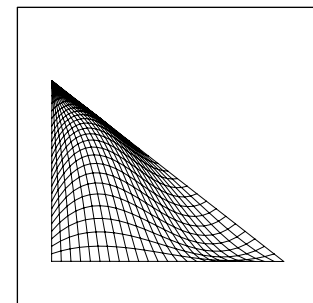


Fig. 5. A bubble function on the reference interface triangle \hat{T} .

A typical example of such bubbles is given in Fig. 5. Checking implication (30) is also elementary here (the reader is referred to [21, p. 181] for further details).

4. Curved interface adaption

In many industrial problems, subdomains correspond to specific substructures with curved interfaces. After finite element discretization, each interface may be represented by different discrete surfaces (Fig. 6). One therefore needs to use a common interface on which the weak continuity constraint will be assembled. In this section, we propose a practical adaption of the mortar method to this framework, relying on the local Hermite patch reconstruction proposed by Puso [28]. Note the present reconstruction gains in locality.

4.1. Modified mortar constraint

Let us now consider a partition $(\Omega_k)_{1 \leq k \leq K}$ of Ω such that the interfaces are curved and piecewise C^1 . Denoting by \mathcal{S} the reunion of these interfaces, we consider a partition $(\Gamma_m)_{1 \leq m \leq M}$ of \mathcal{S} into C^1 manifolds. After independent discretizations of the subdomains, each Ω_k is replaced by a $\Omega_{k;h_k}$ and each Γ_m by two faceted surfaces $\Gamma_{m;\delta_m}^-$ and $\Gamma_{m;\delta_m}^+$ (Fig. 6). Additionally, we assume that $\Gamma_{m;\delta_m}^-$ is an entire number of element faces in the mesh $\mathcal{T}_{k(m);h_{k(m)}}$ on the boundary of $\Omega_{k(m);h_{k(m)}}$.

Assume now we have reconstructed an intermediary interface $\tilde{\Gamma}_{m;\delta_m}^-$. The mortar constraint assembled on this new interface would read for every $1 \leq m \leq M$,

$$\int_{\tilde{\Gamma}_m^-} (\mathfrak{P}u_h^+(\tilde{x}) - \mathfrak{Q}u_h^-(\tilde{x})) \cdot \mathfrak{Q}\mu_\delta(\tilde{x}) d\tilde{s}(\tilde{x}) = 0 \quad \forall \mu_\delta \in M_{m;\delta_m}. \quad (31)$$

Above, u_h^+ , u_h^- denote the discrete displacement fields on the mortar and non-mortar domains $\Omega_{k(m);h_{k(m)}}$, $\Omega_{k(m);h_{k(m)}}$ respectively, as defined in the previous sections. The space $M_{m;\delta_m}$ of Lagrange multipliers is defined on the non-mortar interface $\Gamma_{m;\delta_m}^-$. The two operators \mathfrak{P} and \mathfrak{Q} extend dis-

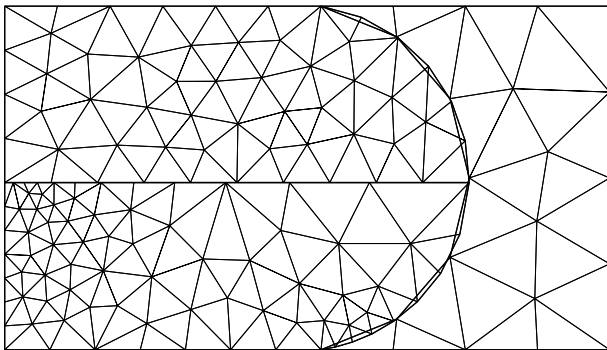


Fig. 6. A geometrically non-conforming decomposition of a domain with curved interfaces.

placements and Lagrange multipliers onto $\tilde{\Gamma}_{m;\delta_m}$, and $d\tilde{s}$ stands for the surface measure over $\tilde{\Gamma}_{m;\delta_m}$.

Of course, the simplest version would be to use directly the faceted non-mortar interface to assemble the constraint, i.e. $\tilde{\Gamma}_{m;\delta_m} = \Gamma_{m;\delta_m}^-$, and to project data onto it face by face. Observe that in general, such a mapping from the mortar side to the non-mortar side is not into. In the following sections, we introduce a more sophisticated formulation, whose interest will appear in the numerical validation.

4.2. Hermite patch reconstruction

In the present section, we propose specific choices to implement practically the generic formulation (31). The regular interface $\tilde{\Gamma}_{m;\delta_m}$ construction is detailed as well as the associated operators \mathfrak{P} and \mathfrak{Q} .

4.2.1. Interface definition

At the nodes located on the boundary of each curved interface $\Gamma_{m;\delta_m}^-$, we first build normal outward unit vectors $n(a)$ approximating the normal on the underlying C^1 surface Γ_m . For every interface $1 \leq m \leq M$ and every internal node $a \in \Gamma_{m;\delta_m}^- \setminus \partial \Gamma_{m;\delta_m}^-$ inside this interface, we then define a normal outward unit vector $n(a)$, say by a weighted averaging process. For instance, denoting by $\mathfrak{F}(a)$ the set of faces in $\Gamma_{m;\delta_m}^-$ sharing the node a , one can use the following average

$$n(a) = \frac{\sum_{F \in \mathfrak{F}(a)} |F| n_F(a)}{\left\| \sum_{F \in \mathfrak{F}(a)} |F| n_F(a) \right\|_2},$$

where $|F|$ is the area of F and n_F the field of its outward normal unit vectors.

Once we have reconstructed the normal unit vectors at each node of the curved interface, we build a regularized interface $\tilde{\Gamma}_{m;\delta_m}^-$ associated to the non-mortar side $\Gamma_{m;\delta_m}^-$ through a mapping $\varphi_m : \Gamma_{m;\delta_m}^- \rightarrow \tilde{\Gamma}_{m;\delta_m}^-$. More precisely, $\tilde{\Gamma}_{m;\delta_m}^-$ is a C^1 manifold and is such that $\varphi_m(a) = a$ for every node $a \in \Gamma_{m;\delta_m}^-$ and such that the normal outward unit vector to $\tilde{\Gamma}_{m;\delta_m}^-$ at a is the vector $n(a)$ constructed above.

Let us detail the expression of φ_m on the face F located on $\Gamma_{m;\delta_m}^-$; F is a face of the element K belonging to $\mathcal{T}_{k(m);h_{k(m)}}$. Let \hat{K} be the associated reference element and $\psi_K : \mathbb{R}^3 \rightarrow \mathbb{R}^3$ the iso-parametric mapping such that $\psi_K(\hat{K}) = K$. Let φ_m be the map defined as

$$\varphi_m \circ \psi_K(\hat{x}) = \psi_K \circ \mathcal{H}_F(\hat{x}) \quad \forall \hat{x} \in \hat{F}, \quad (32)$$

where $\mathcal{H}_F : \hat{F} \rightarrow \mathbb{R}^3$ is a high order mapping to be defined below on the reference element. For every node \hat{a} of \hat{F} , we impose

$$\mathcal{H}_F(\hat{a}) = \hat{a}, \quad (33)$$

so that for every node $a = \psi_K(\hat{a})$ we obtain $\varphi_m(a) = a$. Next, let

$$t_i(a) = \frac{\partial \psi_K}{\partial \hat{x}_i}(\hat{a}), \quad i \in \{1, 2\},$$

be two tangent vectors on F at the node a . We modify them to make them orthogonal to the imposed normal vector $n(a)$; one obtains:

$$\tilde{t}_i(a) = t_i(a) - t_i(a) \cdot n(a) \quad n(a) \quad i \in \{1, 2\}.$$

Due to (32), we deduce the tangent conditions to impose on the local map $\mathcal{H}_F(\hat{x})$ as

$$\frac{\partial \mathcal{H}_F}{\partial \hat{x}_i}(\hat{a}) = \left(\frac{\partial \psi_K}{\partial \hat{x}}(\hat{a}) \right)^{-1} \cdot \tilde{t}_i(\hat{a}) =: \hat{t}_i(\hat{a}) \quad i \in \{1, 2\}. \quad (34)$$

The above construction is illustrated in Fig. 7.

When $\hat{F} = [-1, 1]^2$ is the reference square represented in Fig. 8, \mathcal{H}_F is defined as the Hermite interpolation without twist (as proposed in [28]) and is explicitly given when enforcing (33), (34) as

$$\begin{aligned} \mathcal{H}_F(\hat{x}) = & \zeta(\hat{x}) + \hat{t}_1^1 \theta_1(\hat{x}_1) \phi_1(\hat{x}_2) + \hat{t}_1^2 \theta_2(\hat{x}_1) \phi_1(\hat{x}_2) \\ & + \hat{t}_2^1 \theta_2(\hat{x}_1) \phi_2(\hat{x}_2) + \hat{t}_2^4 \theta_1(\hat{x}_1) \phi_2(\hat{x}_2) \\ & + \hat{t}_2^1 \phi_1(\hat{x}_1) \theta_1(\hat{x}_2) + \hat{t}_2^2 \phi_2(\hat{x}_1) \theta_1(\hat{x}_2) \\ & + \hat{t}_2^3 \phi_2(\hat{x}_1) \theta_2(\hat{x}_2) + \hat{t}_2^4 \phi_1(\hat{x}_1) \theta_2(\hat{x}_2), \end{aligned}$$

where $\hat{t}_i^j = \hat{t}_i(\hat{a}^j)$. The following Hermite interpolation functions have been used:

$$\begin{aligned} \phi_1(s) &= \frac{1}{4}(s-1)^2(2+s), \quad \phi_2(s) = \frac{1}{4}(s+1)^2(2-s), \\ \theta_1(s) &= \frac{1}{8}(s+1)(1-s)^2, \quad \theta_2(s) = \frac{1}{8}(s-1)(1+s)^2, \end{aligned}$$

for every $s \in [-1, 1]$, and for every $\hat{x} \in \hat{F}$,

$$\zeta(\hat{x}) = \frac{1}{2} \begin{pmatrix} \hat{x}_1(3 - |\hat{x}_1|^2) \\ \hat{x}_2(3 - |\hat{x}_2|^2) \end{pmatrix}.$$

If the reference surface element \hat{F} is the triangle represented in Fig. 9, \mathcal{H}_F is given by

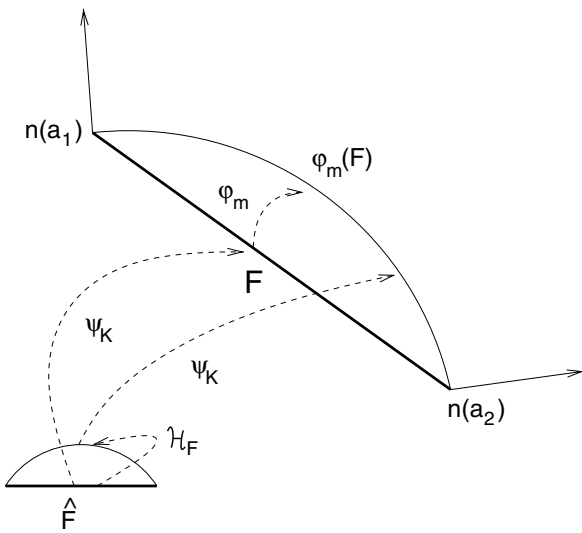


Fig. 7. Interface regularization acting on the 1D interface element F based upon the predicted normal vectors at vertices. \hat{F} denotes the reference element. Illustration of the mappings previously defined.

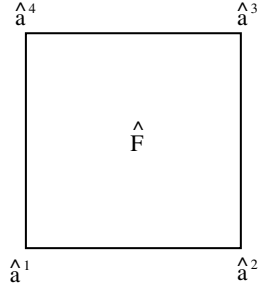


Fig. 8. A square surface reference element $\hat{F} = [-1, 1]^2$.

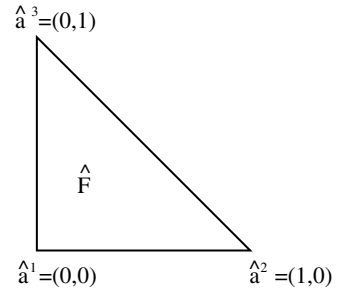


Fig. 9. A triangular surface reference element \hat{F} .

$$\mathcal{H}_F(\hat{x}) = \zeta(\hat{x}) + \sum \hat{t}_1^i S_i(\hat{x}) + \sum \hat{t}_2^i T_i(\hat{x}),$$

where $\hat{t}_i^j = \hat{t}_i(\hat{a}^j)$. The shape functions used in this expression are

$$\begin{cases} S_1(x, y) = x - 2x^2 - xy^2 + x^3 \\ S_2(x, y) = -x^2 + x^3 \\ S_3(x, y) = 2xy - xy^2 - 2x^2y \end{cases} \quad \begin{cases} T_1(x, y) = y - 2y^2 - yx^2 + y^3 \\ T_2(x, y) = 2xy - x^2y - 2xy^2 \\ T_3(x, y) = -y^2 + y^3, \end{cases} \quad (35)$$

and for every $\hat{x} \in \hat{F}$,

$$\zeta(\hat{x}) = \begin{pmatrix} 3|x_1|^2 - 2|\hat{x}_1|^3 \\ 3|x_2|^2 - 2|\hat{x}_2|^3 \end{pmatrix}.$$

4.3. Spaces and projections

The space $M_{m;\delta_m}$ of Lagrange multipliers in (31) is defined as in the plane interface case, on the non-mortar interface $\Gamma_{m;\delta_m}^-$. The projection operator \mathfrak{Q} is defined for every $\tilde{x} \in \tilde{\Gamma}_m$, by

$$\mathfrak{Q}w(\tilde{x}) = w(\varphi_m^{-1}(\tilde{x})).$$

The projection operator \mathfrak{P} obeys for every $\tilde{x} \in \tilde{\Gamma}_m$,

$$\mathfrak{P}w(\tilde{x}) = w(\mathfrak{P}\tilde{x});$$

$\mathfrak{P}\tilde{x} \in \Gamma_{m;\delta_m}^+$ is such that $\tilde{x} - \mathfrak{P}\tilde{x}$ is colinear to the vector $n(\tilde{x})$ normal to $\tilde{\Gamma}_m$ at \tilde{x} .

4.4. Quasi-exact integration

Quadrature approximation of the mortar weak-continuity constraint is known to alter the optimality of the

method [16,26]. Consequently, in spite of the difficulty in handling numerically the surface integrals in (31), one has to compute them “as exactly as possible”. To do so, the expression (31) is splitted into contributions of the faces $F \in \mathcal{F}_{m;\delta_m}$ on the non-mortar side $\Gamma_{m;\delta_m}^-$, as

$$\begin{aligned} & \int_{\Gamma_m^-} (\mathfrak{P}u_h^+(\tilde{x}) - \mathfrak{Q}u_h^-(\tilde{x})) \cdot \mathfrak{Q}\mu_\delta(\tilde{x}) d\tilde{s}(\tilde{x}) \\ &= \sum_{F \in \mathcal{F}_{m;\delta_m}} \int_{\varphi_m(F)} (\mathfrak{P}u_h^+(\tilde{x}) - \mathfrak{Q}u_h^-(\tilde{x})) \cdot \mathfrak{Q}\mu_\delta(\tilde{x}) d\tilde{s}(\tilde{x}) = 0 \\ & \forall \mu_\delta \in M_{m;\delta_m}. \end{aligned}$$

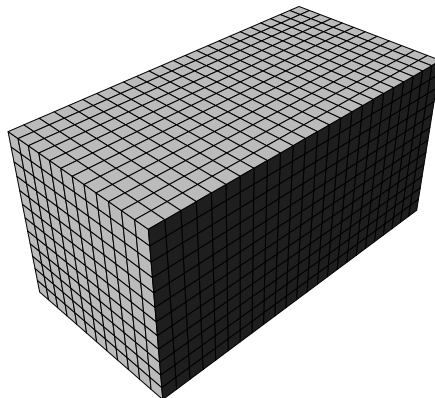
We simply detail the non-conforming contribution, decomposed as follows:

$$\begin{aligned} & \int_{\varphi_m(F)} \mathfrak{P}u_h^+(\tilde{x}) \cdot \mathfrak{Q}\mu_\delta(\tilde{x}) d\tilde{s}(\tilde{x}) \\ &= \sum_{G \subset \Gamma_{m;\delta_m}^+} \int_{\mathfrak{P}G \cap \varphi_m(F)} \mathfrak{P}u_h^+(\tilde{x}) \cdot \mathfrak{Q}\mu_\delta(\tilde{x}) d\tilde{s}(\tilde{x}), \end{aligned}$$

where the sum is over the mortar faces G whose projection $\mathfrak{P}G$ intersects the curved face $\varphi_m(F)$. To compute each integral, we first identify every node b_i of the original mortar face G facing the non-mortar face F , and compute its projection $\mathfrak{P}(b_i) \in \tilde{\Gamma}_{m;\delta_m}^-$ on the curved interface, together with its coordinates $\hat{b}_i = (\psi_K \circ \mathcal{H}_F)^{-1}(b_i)$ in the reference

Young modulus E	5000 Pa
Poisson coefficient ν	0.2
density ρ	1 kg/m ³
traction pressure p	10000 Pa
length L	2 m
thickness l	1 m
extension under static loading	3.97 m
period of the first extensional eigenmode	0.1125 s

Fig. 10. Characteristics of the beam and first numerical estimations.



face \hat{F} . The \hat{b}_i are the vertices of a polygon $\hat{G} \subset \mathbb{R}^2$ intersecting \hat{F} . We will in fact approximate the domain of integration $\mathfrak{P}G \cap \varphi_m(F)$ as the image of $(\hat{F} \cap \hat{G})$ by the map $\psi_K \circ \mathcal{H}_F$, see (32), i.e.

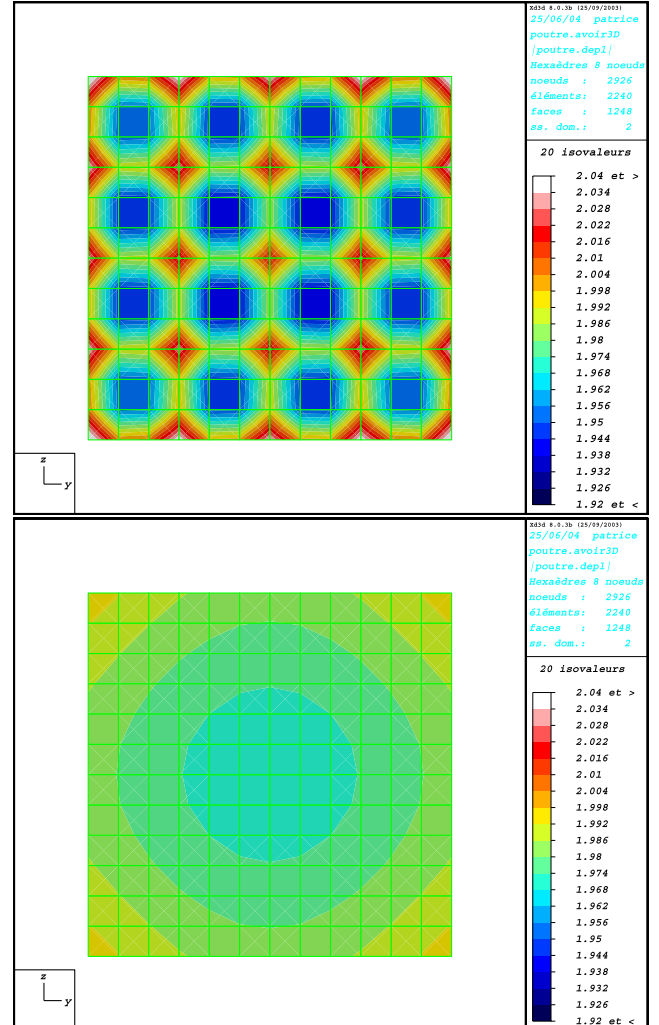


Fig. 12. Interface displacements on the finer side, when using a quadrature approximation (top) and the exact integration (bottom) of the mortar constraint.

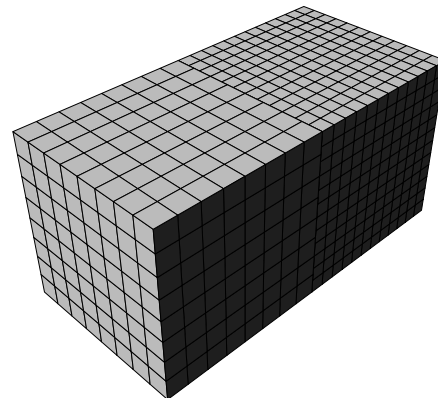


Fig. 11. Conforming (4225 nodes, 3456 elements) and non-conforming (2926 nodes, 2240 elements) meshes of a beam using first-order elements.

$$\mathfrak{P}G \cap \varphi_m(F) \simeq \psi_K \circ \mathcal{H}_F(\hat{F} \cap \hat{G}).$$

Thus, each local contribution can be evaluated on the reference polygon $\hat{F} \cap \hat{G}$ as

$$\begin{aligned} & \int_{\mathfrak{P}G \cap \varphi_m(F)} \mathfrak{P}u_h^+(\tilde{x}) \cdot \mathfrak{Q}\mu_\delta(\tilde{x}) d\tilde{s}(\tilde{x}) \\ & \simeq \int_{\hat{F} \cap \hat{G}} \mathfrak{P}u_h^+(\psi_K \circ \mathcal{H}_F(\hat{x})) \cdot \mu_\delta(\psi_K(\hat{x})) m(\hat{x}) d\hat{x}_1 d\hat{x}_2, \quad (36) \end{aligned}$$

using the metric defined by the curvilinear map $\psi_K \circ \mathcal{H}_F$

$$m(\hat{x}) = \left\| \prod_{i=1}^2 \frac{\partial \psi_K}{\partial x}(\mathcal{H}_F(\hat{x})) \cdot \frac{\partial \mathcal{H}_F}{\partial \hat{x}_i}(\hat{x}) \right\|_2.$$

The polygonal face $\hat{G} \cap \hat{F}$ is the intersection of two polygons in \mathbb{R}^2 , which can be computed using [27] and the routines available on the author's website after suitable modifications. Then, the integral (36) can be computed

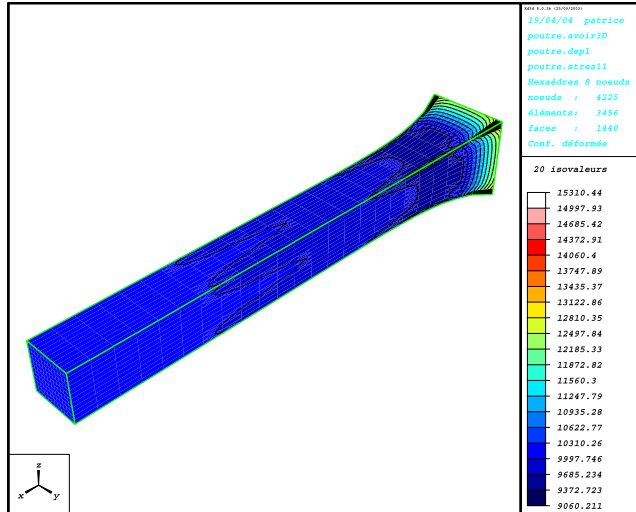
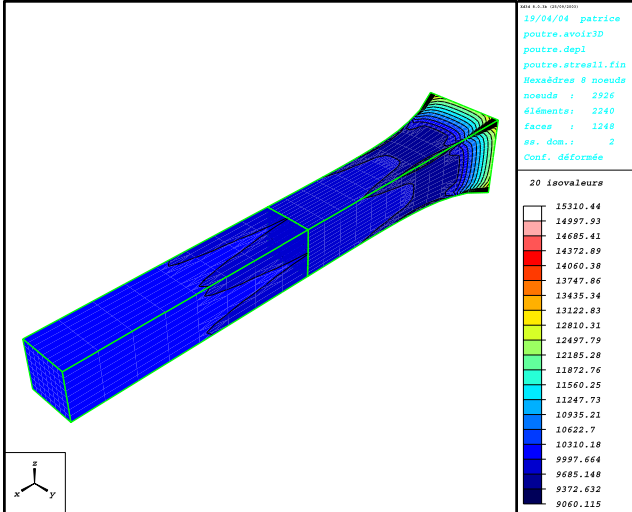


Fig. 13. Distribution of σ_{11} stresses on the deformed configuration of the non-conforming (top) and conforming (bottom) models, by using a first-order approximation for the displacements.

with high accuracy by decomposing the obtained N -polygon $\hat{G} \cap \hat{F}$, into N triangles sharing its barycenter. The integral over each triangle is computed by quadrature using a sufficiently high number of Gauss points – we have used up to 12 Gauss points – since the integrand is not polynomial.

5. Numerical tests for discontinuous mortar-elements

5.1. Beam under traction

First, we consider an homogeneous beam made of an isotropic elastic material, whose a tip is clamped on a wall. The free tip is subjected to a uniform negative pressure. All the characteristics are detailed in the table, Fig. 10. For comparison purpose, non-conforming and conforming meshes are considered, as shown in Fig. 11.

Displacements are approximated by \mathbb{Q}_1 first-order finite elements enriched with a bubble interface stabilization on

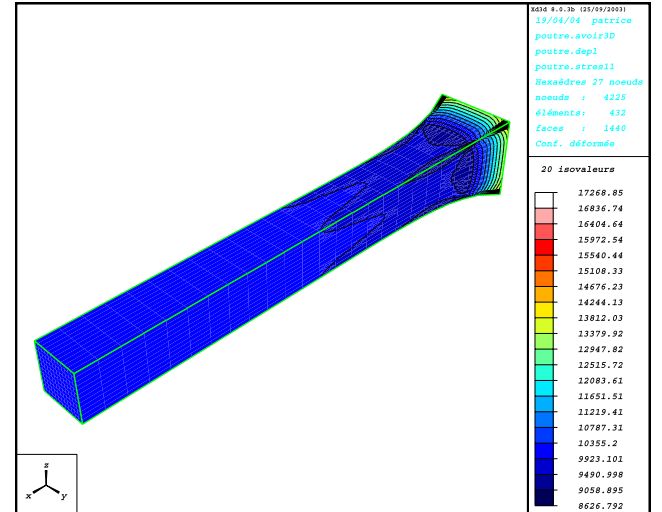
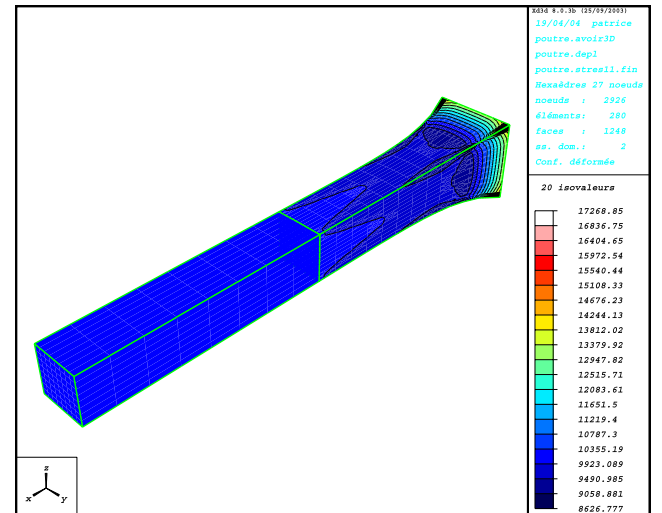


Fig. 14. Distribution of σ_{11} stresses on the deformed configuration of the non-conforming (top) and conforming (bottom) models, by using a second-order approximation for the displacements.

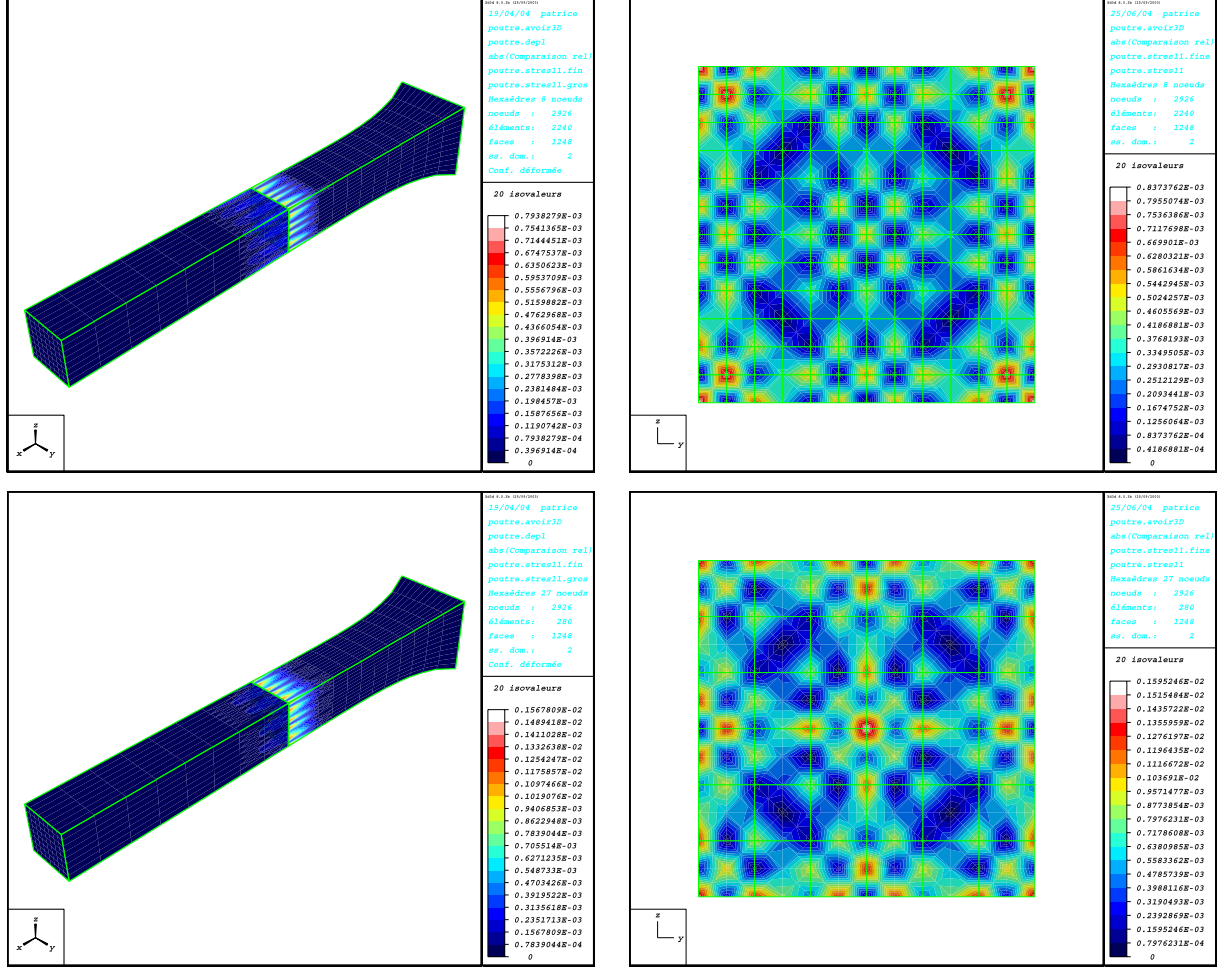


Fig. 15. Relative gap of σ_{11} stresses between the solutions computed on the non-conforming model for the two possible choices of the non-mortar side, when using a first-order (top) and a second-order (bottom) approximation for the displacements. The pictures on the right column are zooms on the finer side of the interface. The relative gap remains smaller than 8.4×10^{-4} (resp. 1.6×10^{-3}) for the first-order (resp. second-order) approximation.

the finer side, which will be the non-mortar side of the interface. As described in Section 3.1, Lagrange multipliers are chosen piecewise-constant on the non-mortar side.

We start by illustrating the non-optimal results obtained when computing the mortar constraint by quadrature on the finer side of the interface. Such a computation using an inexact quadrature rule of the mortar surface integral leads to interface oscillations of the displacements, as shown in Fig. 12. This result confirms the work of [16,26].

When using now exact quadrature for the mortar integrals, the error in displacements between the conforming and non-conforming models is about 5×10^{-6} m in L^∞ norm. The corresponding relative error is about 10^{-6} . Concerning Cauchy stresses, a 4×10^{-4} relative gap between the conforming and non-conforming models is observed. This very good agreement is illustrated in Fig. 13, where the computed distribution of σ_{11} stresses is represented.

Finally, let us discuss the influence of the choice of the non-mortar side (defining the multipliers either on the

coarse side, or on the fine one) on the solution. The relative gap of the displacements (resp. of the σ_{11} stresses) in L^∞ norm between the non-conforming solutions computed with these choices is 2×10^{-6} (resp. 8×10^{-4}). As illustrated in Fig. 15, the relative gap of stresses remains concentrated on the elements sharing the interface. These relative gaps comparing the solutions associated with different non-mortar sides have the same amplitude than the relative gaps between the conforming and non-conforming solutions. Therefore, the static analysis is confirmed (at least in a homogeneous model), indicating that the choice of the non-mortar side can be made arbitrarily without affecting optimality.

The same simulations have been computed for a \mathbb{Q}_2 approximation of the displacements both on conforming and non-conforming models, using the interface stabilization presented in Section 3.2, and discontinuous \mathbb{P}_1 Lagrange multipliers. For this second-order approximation, we have kept the same number of nodes as in the previous first-order approximation. The relative gap in displacements (resp. maximal stresses) in L^∞ norm

between conforming and non-conforming models is 3×10^{-6} (resp. 1×10^{-3}). The distribution of σ_{11} stresses for the conforming and non-conforming models is represented in Fig. 14. Moreover, we show in Fig. 15 that the influence of the choice of the non-mortar side (defining the multipliers either on the coarse side, or on the fine one) is again rather small in this case. Indeed, the relative gap for the σ_{11} stresses between the solutions for the two possible choices of the non-mortar side is always smaller than 2×10^{-3} , keeping the same amplitude than the gap in stresses between the conforming and non-conforming solutions. It is worth noticing that whereas the relative gap for displacements between the first and second-order models is 2×10^{-4} in L^∞ norm, the maximal stress has been increased by 10 in the second-order model, due to

the presence of a singularity at the corners of the fixed tip of the beam.

Let us now consider the elastodynamics problem associated with the previous beam model, by using the trapezoidal time discretization given by (7). For comparison purpose, the first order conforming and non-conforming space discretizations used above in the static case are tested. Here, the non-mortar side is the finer one. A constant traction (identical to the static case) is applied at the tip of the beam. As this sollicitation is derived from a potential, oscillations are expected and observed. Some snapshots of the computed dynamics are given in Fig. 16. In order to compare the space non-conforming solution with the conforming one, the horizontal displacement of the central node of the free tip of the beam is represented

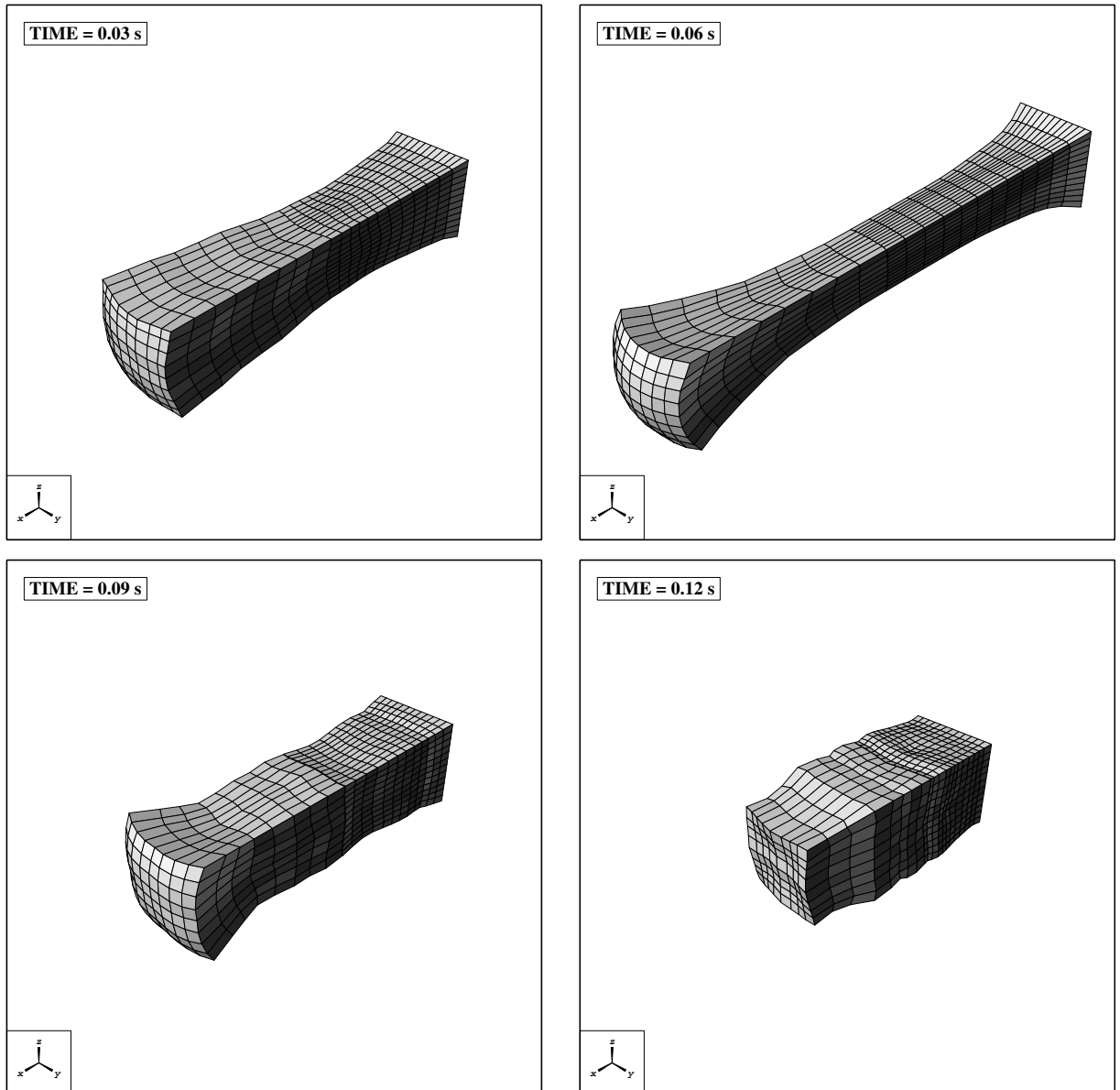


Fig. 16. Snapshots of the computed dynamics of the beam by using a non-conforming first-order approximation of the displacements.

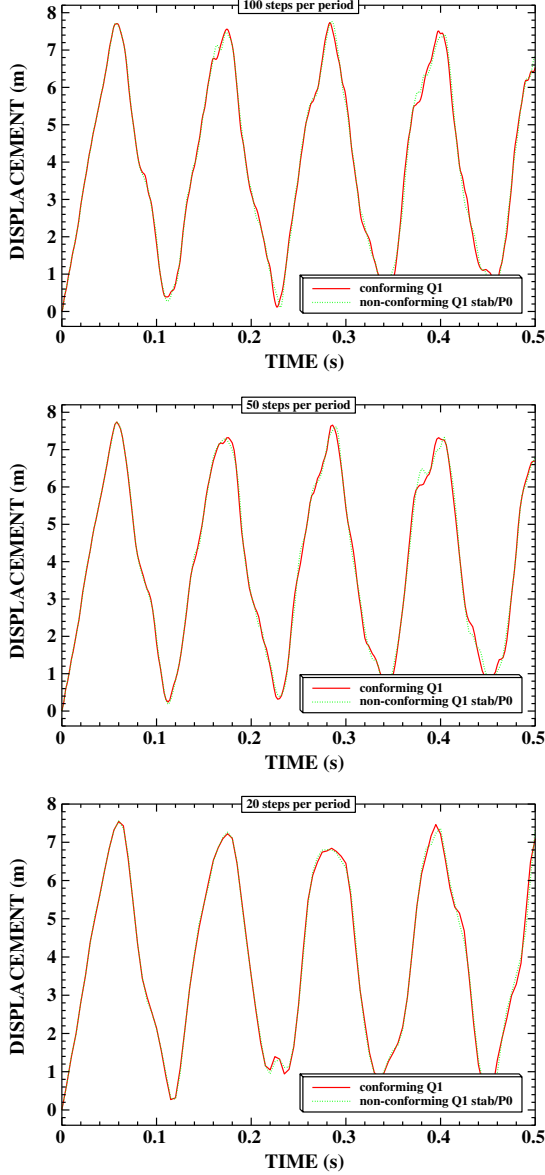


Fig. 17. Horizontal displacement of the central node of the tip of the beam as a function of time, both for the non-conforming and conforming first-order space approximation of the beam, together with a trapezoidal approximation in time. Simulations done with 20, 50 and 100 time steps per period. The good agreement confirms the optimality of the non-conforming space approximation.

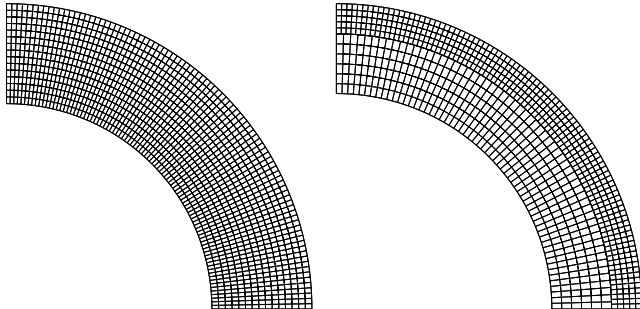


Fig. 18. Conforming (1456 nodes, 1350 elements) and non-conforming (973 nodes, 810 elements) meshes of a cylinder in plane displacements.

in Fig. 17 both for non-conforming and conforming approximations when using 20, 50 and 100 time steps per oscillation period. The solutions are very close from each other, which confirms the theoretical result of optimality for our space non-conforming approximation in linear elastodynamics.

Young modulus E	5000 Pa
Poisson coefficient ν	0.2
internal pressure p	100 Pa
internal radius	1.0 m
interface radius	1.33 m
external radius	1.5 m
maximal displacement under loading	0.058 m

Fig. 19. Characteristics of the cylinder.

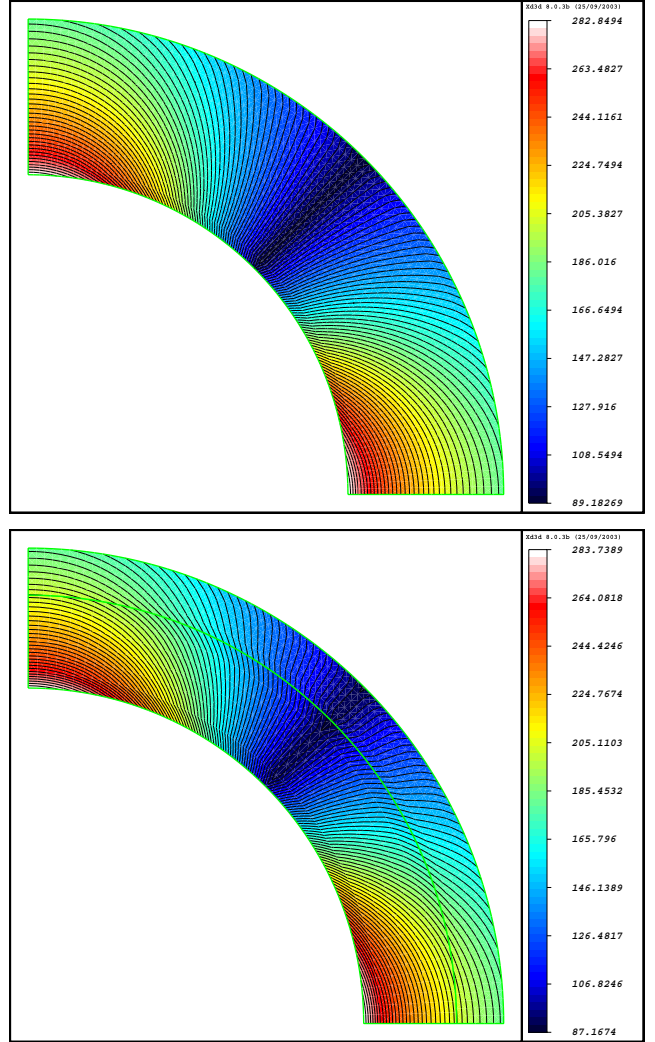


Fig. 20. Distribution of the maximal stresses in a cylinder under pressure both for conforming and non-conforming space approximation.

5.2. Cylinder in plane displacements

An homogeneous bidimensional cylinder in plane displacements under pressure load is considered. This prob-

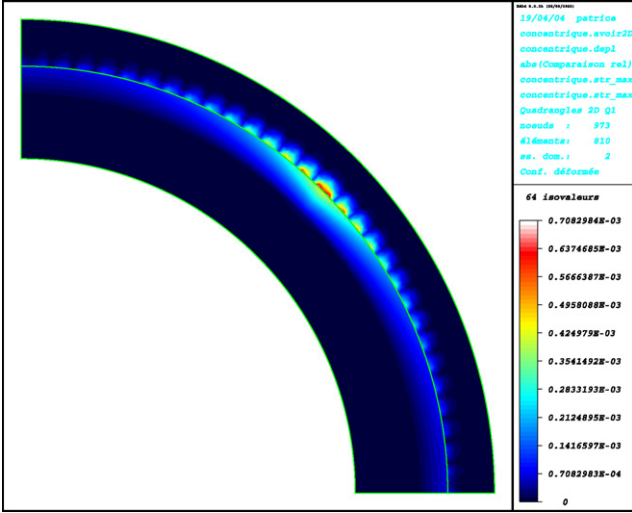


Fig. 21. Relative gap of the σ_{11} stresses between the solutions computed on the non-conforming model for the two possible choices of the non-mortar side, when using a stabilized first-order approximation for the displacements and piecewise constant Lagrange multipliers. The relative gap remains smaller than 7.1×10^{-4} .

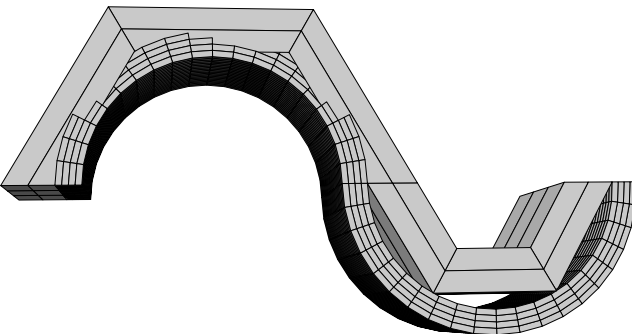


Fig. 22. A two-layer problem with incompatible meshes.

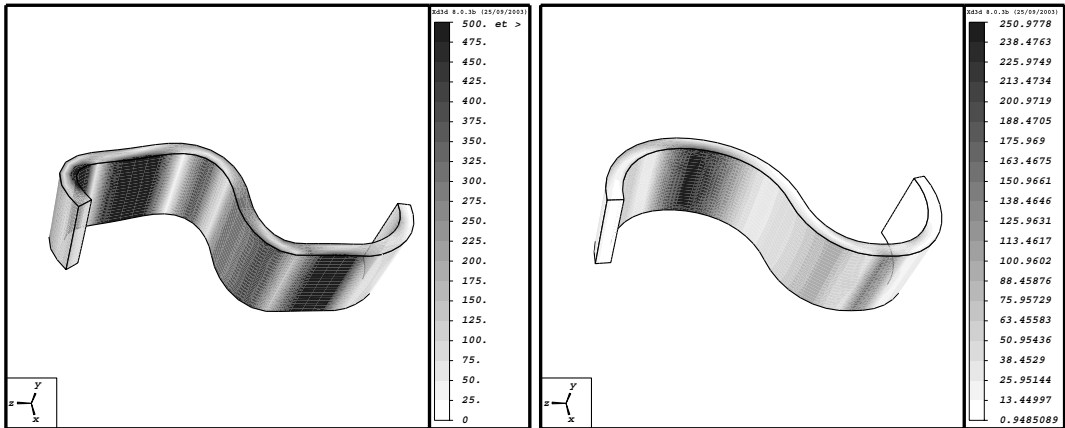


Fig. 23. Stress distribution over the deformed configuration for the finer layer. The non-mortar side is the coarser and the results show the effect of the interface regularization (right) as compared to the standard approach (left).

lem involves a curved interface. The cylinder is made of an isotropic linearly elastic material whose characteristics are given on the table, Fig. 19. As previously, for comparison purpose, we consider conforming and non-conforming meshes, as shown in Fig. 18. As presented in Section 3.1, the displacements are approximated by \mathbb{Q}_1 polynomials supplemented by a bubble interface stabilization; Lagrange multipliers are piecewise constant. In this case, the non-mortar and mortar interfaces do not geometrically match. To formulate the weak-continuity constraint, the approach from Section 4 is used. The distribution of maximal stresses over the deformed configuration is represented in Fig. 20, both for conforming and non-conforming first-order approximations. The quality of the non-conforming approximation shows here the small influence of the geometric non-conformity. The influence of the choice of the non-mortar side is also studied, and the relative gap of the maximal stresses between the two possible choices is represented in Fig. 21. Because of the homogeneity of the material and because the non-conforming interface is not in a high stress region, such an influence remains very small.

5.3. Interface regularization

One may legitimately wonder if the interface regularization proposed above is able to improve convergence order. As a matter of fact, we are not able to show that asymptotically, the convergence order with respect to the mesh-size is improved. Nevertheless, practice shows that for nonlinear problems involving contact and incompatible meshes having very different mesh sizes, the regularity of the stress distribution is improved, especially when some of the meshes remain quite coarse. For some complex problems of industrial interest, such regularization even improves the Newton method convergence.

Let us consider the case of a layered structure made of two waves built with the same material. The top one has the coarser mesh, and the two layers are glued using the

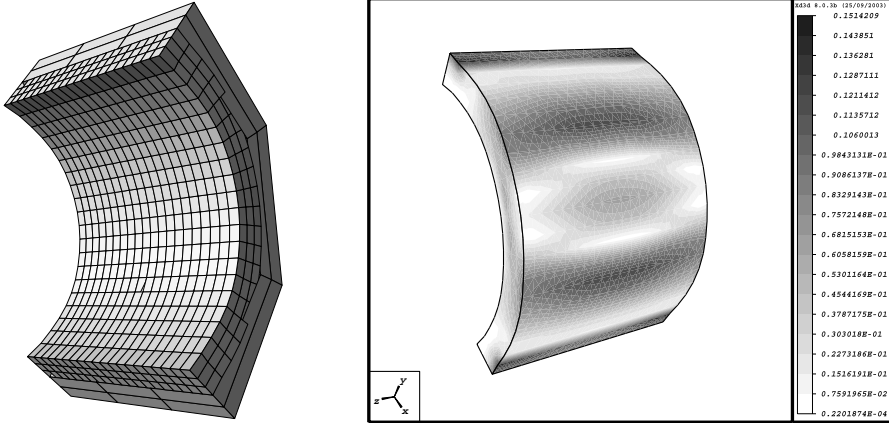


Fig. 24. Left: Two-layer quarter of cylinder with incompatible meshes. Right: Relative gap of maximal stresses between the solutions with and without interface regularization.

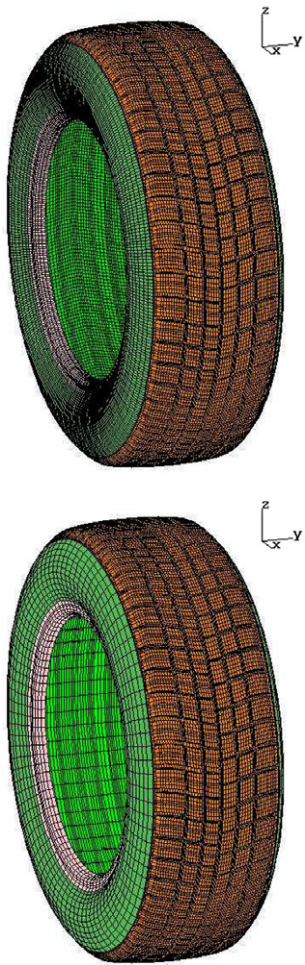


Fig. 25. Compatible and incompatible meshes of a tire. The incompatible mesh has an incompatibility ratio of 4 approximatively (i.e. the fine mesh has about 4 times more elements on the interface).

mortar method. The whole structure is forced to enter in frictionless contact with a plane ground below the finer layer. The underformed structure is shown in Fig. 22.

The stress distribution over the deformed configuration is displayed in Fig. 23; the non-mortar side is the coarser. In the absence of the proposed modification, the displacement field on the finer layer lacks regularity and exhibits high local stresses.

This result notwithstanding, we have observed that in the absence of contact for instance, i.e. for smoother problems, the improvement brought by the presented technique is less obvious. For instance, let us consider a quarter of cylinder made of two layers of identical materials; it is clamped at its tips and an internal pressure is applied. The solutions with and without regularization are extremely similar in terms of displacements; stresses differ by less 15%, as illustrated in Fig. 24.

5.4. Industrial computation in tire industry

The work presented herein has also been used to compute with success an industrial test case in nonlinear elasticity and large deformations, reproduced herein by courtesy of Michelin. Let be given a standard tire, two meshes of it being represented in Fig. 25. The displacements on the interface between the architecture and sculptures are glued by using the proposed discontinuous mortar formulation, using the reconstructed curved interfaces.

When the wheel experiences a vertical load at its center, the tire undergoes a static deformation. The corresponding contact pressures on a plane ground are represented in Fig. 26 for compatible and incompatible meshes. Such an illustration shows the very good agreement between conforming and non-conforming computations and confirms the optimality of the mortar approximation (Part 1), even in the nonlinear framework.

In addition, when the center of the wheel is submitted to a 1 km/h horizontal velocity, the unsteady contact pressures computed on the conforming and non-conforming models prove again to be very close, as illustrated in Fig. 27.

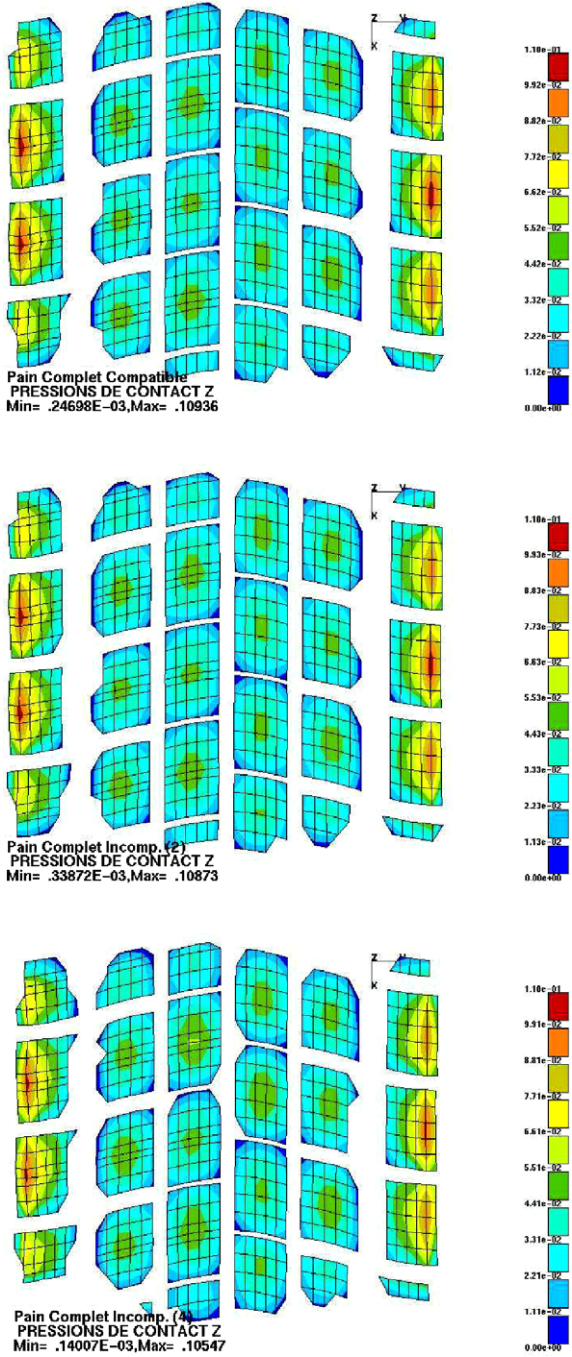


Fig. 26. Contact pressures obtained respectively for the compatible mesh (top), and incompatible meshes with incompatibility ratios of 2 (middle) and 4 (bottom).

The interest of such a test case is to indicate that the mortar formulation also applies well to large industrial computations, and that the optimal results shown herein in the linearized framework seem to extend perfectly to the nonlinear case.

6. Conclusion

This paper has shown the optimal extension of the mortar method to linearized elastodynamics, and has intro-

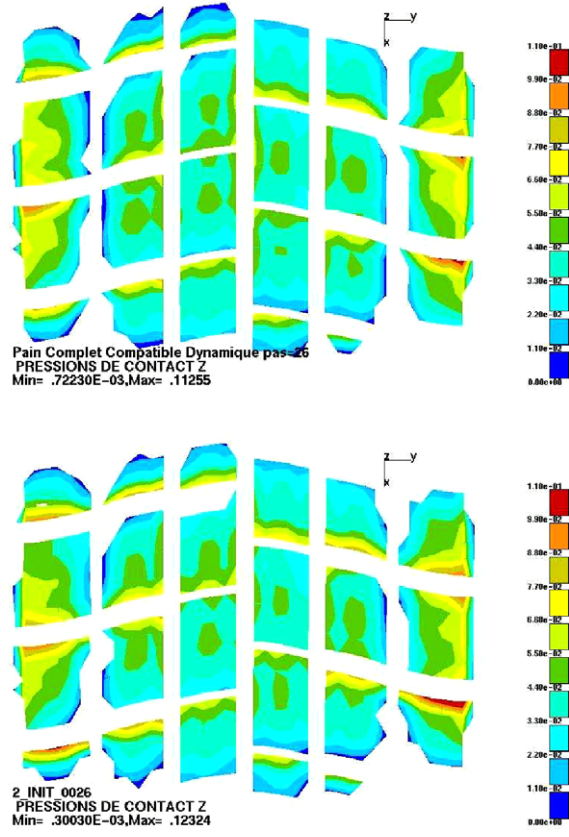


Fig. 27. Contact pressures for the 1 km/h unstationary rolling of the tire, computed on a compatible mesh (top) and an incompatible mesh with an incompatibility ratio of 4 (bottom).

duced, analyzed and tested a discontinuous stabilized formulation. The formulation avoids the usual special treatment of cross points and cross lines, and renders the coupling block diagonal. The issue of curved-interface treatment has been addressed from the practical point of view, and numerical examples confirm the efficiency of the method for nonlinear industrial problems.

Acknowledgements

P.H. would like to gratefully acknowledge the support of Michelin Tire Company during the completion of his Ph.D. work at the Center of Applied Mathematics (CMAP), Ecole Polytechnique. Moreover, we would like to express our gratitude to Ali Rezgui for his enthusiastic encouragement, and to François Jouve for kindly providing his finite element code, developed at CMAP, Ecole Polytechnique, in which we have implemented the presented ideas.

References

- [1] A. Agouzal, J.M. Thomas, Une méthode d'éléments finis hybrides en décomposition de domaines, RAIRO M2AN 29 (1995) 749–764.
- [2] J.-P. Aubin, Analyse fonctionnelle appliquée, vols. 1 and 2, Presses Universitaires de France, 1987.

- [3] M. Azaïez, F. Ben Belgacem, H. El Fekih, M. Ismaïl, Numerical simulation of the wave equation with discontinuous coefficients by nonconforming finite elements, *Numer. Methods Partial Differ. Eq.* 15 (6) (1999) 637–656.
- [4] I. Babuška, The finite-element method with Lagrangian multipliers, *Numer. Math.* 20 (1973) 179–182.
- [5] F. Ben Belgacem, The mortar finite element method with Lagrange multipliers, *Numer. Math.* 84 (1999) 173–197.
- [6] F. Ben Belgacem, A stabilized domain decomposition method with non-matching grids for the Stokes problem in three dimensions, *SIAM J. Numer. Anal.* 42 (2) (2004) 667–685.
- [7] F. Ben Belgacem, Y. Maday, The mortar element method for three dimensional finite element, *M2AN* 31 (1997) 289–303.
- [8] C. Bernardi, Y. Maday, A.T. Patera, Domain decomposition by the mortar element method, in: H.G. Kaper, M. Garbey (Eds.), *Asymptotic and Numerical Methods for Partial Differential Equations with Critical Parameters*, Kluwer Academic Publishers, N.A.T.O. ASI, 1993, pp. 269–286.
- [9] C. Bernardi, Y. Maday, A.T. Patera, Nonlinear partial differential equations and their applications, Collège de France Seminar XI, A New Nonconforming Approach to Domain Decomposition: The Mortar Element Method, Pitman, Paris, 1994.
- [10] J. Boland, R. Nicolaides, Stability of finite elements under divergence constraint, *SIAM Numer. Anal.* 20 (4) (1983) 722–731.
- [11] J. Boland, R.A. Nicolaides, Stable and semistable low order finite elements for viscous flows, *SIAM J. Numer. Anal.* 22 (1985) 474–492.
- [12] S. Brenner, Poincaré-Friedrichs inequalities for piecewise H^1 functions, *SIAM J. Numer. Anal.* 41 (1) (2003) 306–324.
- [13] S. Brenner, Korn's inequalities for piecewise H^1 vector fields, *Math. Comput.* 73 (2004) 1067–1087.
- [14] F. Brezzi, On the existence, uniqueness and approximation of saddle-point problems arising from Lagrangian multipliers, *RAIRO Anal. Numer. Ser. Rouge* 8 (1974) 129–151.
- [15] F. Brezzi, D. Marini, Error estimates for the three-field formulation with bubble stabilization, *Math. Comput.* 70 (2000) 911–934.
- [16] L. Cazabœuf, C. Lacour, Y. Maday, Numerical quadratures and mortar methods, in: *Computational Science for the 21st Century*, John Wiley and Sons, 1997, pp. 119–128.
- [17] B. Flemisch, J.M. Melenk, B.I. Wohlmuth, Mortar methods with curved interfaces, *Appl. Numer. Math.* 54 (3–4) (2005) 339–361.
- [18] B. Flemisch, M.A. Puso, B. Wohlmuth, A new dual mortar method for curved interfaces: 2d elasticity, *Int. J. Numer. Methods Engrg.* 63 (6) (2005) 813–832.
- [19] B. Flemisch, B.I. Wohlmuth, Stable lagrange multipliers for quadrilateral meshes of curved interfaces in 3d. Technical report, Stuttgart University, July 2005.
- [20] J. Gopalakrishnan, On the mortar finite element method, Ph.D. thesis, Texas A&M University, August 1999.
- [21] P. Hauret, Méthodes numériques pour la dynamique des structures non-linéaires incompressibles à deux échelles (Numerical methods for the dynamic analysis of two-scale incompressible nonlinear structures), Ph.D. thesis, Ecole Polytechnique, 2004.
- [22] S. Hüeber, B.I. Wohlmuth, A primal-dual active set strategy for nonlinear multibody contact problems, *Comput. Methods Appl. Mech. Engrg.* 194 (2005) 3147–3166.
- [23] C. Kim, R.D. Lazarov, J.E. Pasciak, P.S. Vassilevski, Multiplier spaces for the mortar finite element method in three dimensions, *SIAM J. Numer. Anal.* 39 (2001) 519–538.
- [24] O.A. Ladyzhenskaya, *The Mathematical Theory of Viscous Incompressible Flows*, Gordon and Breach, 1969.
- [25] B. Lamichhane, B.I. Wohlmuth, Biorthogonal bases with local support and approximation properties. Technical Report 2005-02, IANS, Stuttgart, 2005.
- [26] Y. Maday, F. Rapetti, B. Wohlmuth, The influence of quadrature formulas in 3d mortar methods, in: *Recent Developments in Domain Decomposition Methods*, Lecture Notes in Computational Science and Engineering, vol. 23, Springer, 2002, pp. 203–221.
- [27] J. O'Rourke, *Computational Geometry in C*, second ed., Cambridge University Press, 1998.
- [28] M.A. Puso, A 3d mortar method for solid mechanics, *Int. J. Numer. Methods Engrg.* 59 (2004) 315–336.
- [29] M.A. Puso, T.A. Laursen, A 3d contact smoothing method using gregory patches, *Int. J. Numer. Methods Engrg.* 54 (2002) 1161–1194.
- [30] M.A. Puso, T.A. Laursen, Mesh tying on curved surfaces in 3d, *Engrg. Comput.* 20 (2003) 305–319.
- [31] P. Seshaiyer, Non-conforming hp finite element methods, Ph.D. thesis, University of Maryland, 1998.
- [32] R. Stenberg, Analysis of mixed finite element methods for the Stokes problem: a unified approach, *Math. Comput.* 42 (1984) 9–23.
- [33] R. Stenberg, Error analysis of some finite element methods for the Stokes problem, *Math. Comput.* 54 (1990) 495–508.
- [34] R. Stenberg, A technique for analysing finite element methods for viscous incompressible flow, *Int. J. Numer. Methods Fluids* 11 (1990) 935–948.
- [35] P. Le Tallec, S. Mani, Numeric analysis of a linearized fluid-structure interaction problem, *Numer. Math.* 87 (2000) 317–354.
- [36] B.I. Wohlmuth, A mortar finite element method using dual spaces for the Lagrange multiplier, *SIAM J. Numer. Anal.* 38 (2000) 989–1012.
- [37] B.I. Wohlmuth, *Discretization Methods and Iterative Solvers Based on Domain Decomposition*, Springer, 2001.